Transportation Research Part D 154 (2026) 105267

Contents lists available at ScienceDirect

Transportation Research Part D

journal homepage: www.elsevier.com/locate/trd

Integrated hierarchical framework for electric vehicle charging infrastructure management

Zi-Xuan Zhou [a], Jiawei Feng [a,b], Haowen Lei [c], Wenjun Mei [a], Yasuo Asakura [d], Kai Liu [e,*]

[a] College of Engineering, Peking University, Beijing, China
[b] Sustainability X-Lab, The University of Hong Kong, Hong Kong, China
[c] Division of Emerging Interdisciplinary Areas (EMIA), Academy of Interdisciplinary Studies, The Hong Kong University of Science and Technology, Hong Kong, China
[d] Department of Civil Engineering, The University of Tokyo, Tokyo, Japan
[e] School of Economics and Management, Dalian University of Technology, Dalian, China

ARTICLE INFO

Keywords:
Charging scheduling
Parking management
Multi-layer optimization
Resource allocation
Reinforcement learning

ABSTRACT

This work presents a hierarchical optimization framework for electric vehicle (EV) charging infrastructure management that integrates spatial layout design, resource allocation, and real-time scheduling. Building upon prior studies that address these problems individually, our framework introduces vertical integration and horizontal coordination to more comprehensively analyze their critical interdependencies. The spatial layer employs integer linear programming with Voronoi-based decomposition, achieving spatial efficiency ratios up to 1.87. The resource allocation layer implements adaptive algorithm selection, dynamically choosing between mixed-integer programming, particle swarm optimization, and rolling horizon heuristics according to problem scale. The scheduling layer utilizes Soft Actor-Critic reinforcement learning with multi-dimensional reward functions for real-time decision-making. Experimental validation on a 2,102-space commercial parking lot demonstrates substantial improvements: 23.7% reduction in vehicle movements, 48.6% reduction in waiting time, and 14.2% reduction in electricity costs. The framework maintains robust performance under operational disruptions, providing a scalable solution for sustainable EV charging infrastructure management.

1. Introduction

The accelerating global transition to electric mobility (Zhao et al., 2024; Zhou et al., 2024), driven by stringent carbon emission reduction targets (Foda and Mohamed, 2026; Wu et al., 2025) and supportive international policies (Mahyari and Freeman, 2025), presents unprecedented challenges for urban transportation infrastructure (Powell et al., 2022), particularly in ensuring adequate power supply systems and charging networks to support the expanding and diversified fleet of electric vehicles (Hiermann et al., 2016). Despite recent advances in battery technology, persistent limitations in capacity and charging efficiency (Meyer et al., 2025) continue to fuel range anxiety (Ghamami et al., 2020), while inefficient and inadequate charging infrastructure has emerged as the most critical bottleneck impeding this transformation. Comparing with conventional refueling systems that evolved over decades (Davis et al., 2018), EV charging infrastructure remains in early stages of development, facing complex operational challenges including extended

* Corresponding author.
E-mail address: liukai@dlut.edu.cn (K. Liu).

https://doi.org/10.1016/j.trd.2026.105267
Received 9 October 2025; Received in revised form 6 February 2026; Accepted 6 February 2026
Available online 18 February 2026

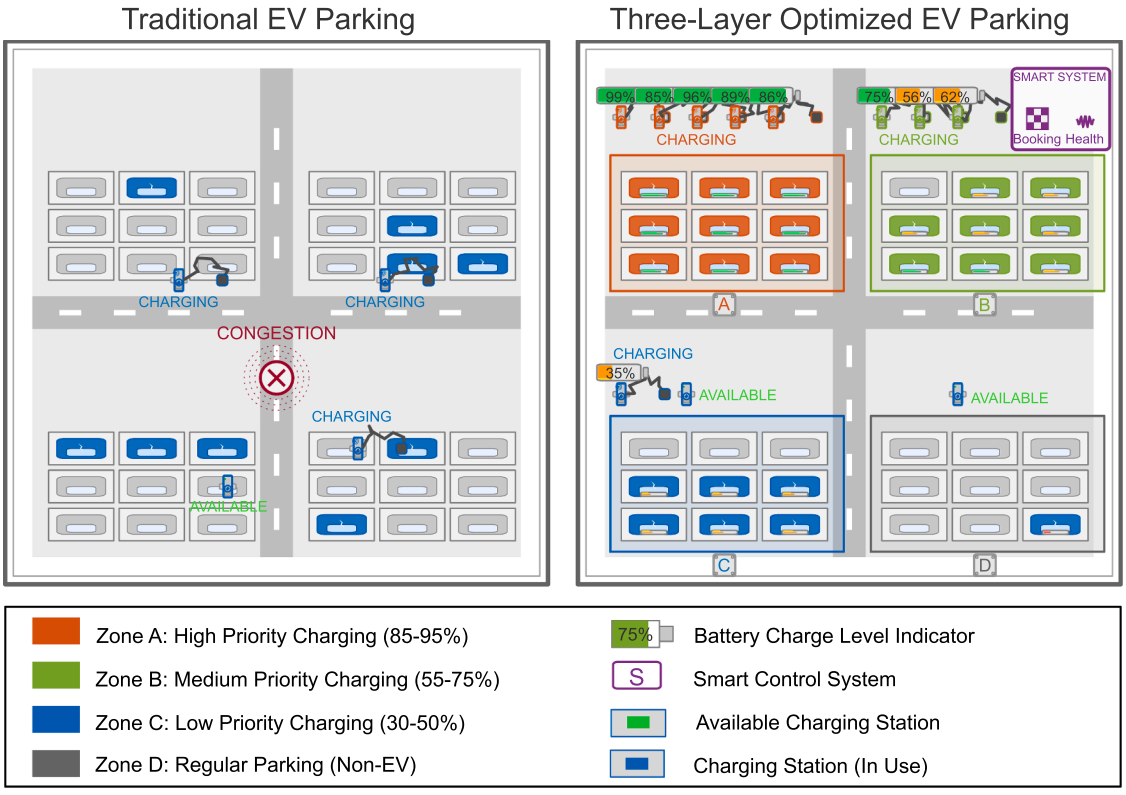

Fig. 1. Comparison of traditional and Multi-Lay1er EV charging management systems.

charging durations (Zhang et al., 2021), limited grid capacity (Iacobucci et al., 2019), and heterogeneous user behaviors (Bae et al., 2024). This infrastructure challenge demands fundamental reconceptualization of how charging resources are spatially distributed (Xu and Meng, 2020), dynamically planning (Sun et al., 2020), and operationally scheduled (He et al., 2020; Zhou et al., 2025).

Regarding the planning of charging stations, past research has done extensive work on site selection (Kinay et al., 2021), route planning (Ghamami et al., 2020), and heterogeneous fleet schedule (Park and Lee, 2024), yet as parking facilities evolve to incorporate charging capabilities, the allocation and management of integrated parking-charging resources has emerged as increasingly critical. Fig. 1 illustrates how traditional EV parking facilities (left panel) exhibit random resource distribution, creating congestion points and underutilized stations without prioritization (Babar and Burtch, 2024), comparing with facility with charging management system. Current EV charging management systems predominantly employ first-come-first-served (FCFS) strategies that fail to leverage the inherent flexibility in charging operations (Xie et al., 2018). These simplistic approaches result in inefficiencies in some scenrios: vehicles with minimal charging needs occupy high-power stations while urgent cases heterogeneity among fleets (Wang and Zhao, 2023), spatial layouts ignore charging demand patterns (He et al., 2022), and resource allocation remains static despite dynamic electricity prices and grid constraints (Yang et al., 2024; Broadbent et al., 2022). While Yang et al. (2021) demonstrated that real-time charging prices based on regional grid load can effectively reduce peak-valley differences by 14.5% and lower users costs by 33.9%, their approach focuses primarily on temporal scheduling without considering spatical constraints or resource allocation challenges. These inefficiencies not only impede EV adoption but also strain electrical grids and increase operational costs for both providers and users.

These challenges mentioned above in EV charging management stems from the interconnected nature of three critical decision domains: spatial layout design (Stephan et al., 2021; Nourinejad et al., 2018), charging resource allocation (Davatgari et al., 2024), and real-time scheduling (Yan et al., 2024). Spatial decisions determine the physical configuration of charging stations within facilities, establishing constraints that persist for years. Resource allocation decisions assign vehicles to charging stations over medium-term horizons, balancing demand with available capacity. Real-time scheduling decisions control power delivery and vehicle movements, responding to immediate operational conditions. Traditional approaches treat these domains independently (Yang et al., 2021), ignoring crucial interdependencies-inappropriate spatial layouts constrain resource allocation flexibility, while suboptimal resource allocation limits scheduling effectiveness.

Existing literature has made notable progress in individual aspects of charging management (An, 2020). Spatial optimization research has focused on station location problems using geographic information systems and accessibility metrics (Tran et al., 2021). Resource allocation studies have employed various optimization techniques including mixed-integer programming and metaheuristics to assign vehicles to stations (Dolgui et al., 2025; Jordán et al., 2022; Tang et al., 2019). Real-time scheduling research has

increasingly adopted reinforcement learning approaches to manage charging operations dynamically (Jin and Xu, 2021; Chen et al., 2025). However, these isolated approaches fail to capture the hierarchical dependencies and feedback loops between decision layers. Consequently, the resulting solutions are often incompatible with complex scenarios and fall short of achieving global optimization across multi-dimensional metrics.

The integration challenge is particularly acute in commercial parking facilities where EVs must share limited space with conventional vehicles while satisfying diverse charging requirements. Unlike dedicated charging stations, parking facilities face additional constraints including vehicle relocation logistics, multi-story layouts, and varying dwell times (Hu et al., 2025a). The complexity intensifies when considering operational uncertainties-equipment failures, demand fluctuations, and price volatility require adaptive responses across all decision layers. Current single-layer optimization methods cannot adequately address these multifaceted challenges, necessitating an integrated approach.

The core innovation of this research lies in the introduction of a hierarchical three-layer optimization framework, which which builds upon prior efforts to systematically integrates the three interdependent decision-making dimensions in EV charging management: spatial layout, resource allocation, and real-time scheduling. Previous research has largely addressed these critical domains in isolation, leading to a significant performance gap. Our work contributes to narrowing this gap by introducing novel mechanisms for both vertical integration (to achieve inter-layer coordination) and horizontal coordination (to optimize intra-layer decisions). This holistic approach enables us to explicitly model and exploit the complex interdependencies ignored by siloed methods. Furthermore, we establish a solid theoretical foundation for this integrated approach, providing convergence guarantees, stability analysis, and performance bounds-a level of analytical rigor absent in prior fragmented solutions.

This unified framework represents a further exploration into enhancing the practical management of EV charging infrastructure. By pursuing near-optimal solutions while maintaining computational tractability, our work offers potential for the development of smarter, more efficient, and more profitable charging facilities. Specifically, validation experiments in a large-scale commercial facility with 2102 spaces suggest that the framework can lead to significant and quantifiable improvements in operational efficiency, user satisfaction, and economic performance. Another key feature is its adaptive computation engine, which dynamically selects the optimal algorithm based on problem scale, a design intended to allow the framework to scale effectively from small private parking lots to large commercial complexes.

The remainder of this paper is organized as follows. Section 2 reviews related literature and identifies research gaps. Section 3 presents the three-layer optimization framework with detailed mathematical formulations. Section 4 develops the solution methodology including advanced algorithmic implementations. Section 5 reports numerical experiments and performance evaluation. Section 6 discusses implications and limitations. Section 7 concludes with future research directions.

2. Literature review

Electric vehicle charging management has evolved from basic timer controls to sophisticated optimization frameworks balancing multiple objectives (Cao et al., 2018). As EV adoption accelerated, research shifted toward efficiency optimization, particularly minimizing costs, maximizing infrastructure utilization, and mitigating grid impacts.

2.1. Charging management

Recent charging management approaches demonstrate diverse innovations. Integration with user behavior proves particularly effective, Habib et al. (2025) achieved 20% peak demand reduction combining station planning with parking behavior, while Xu et al. (2018) reduced grid loads through strategic timing based on urban mobility patterns. Stochastic traffic conditions significantly affect electric bus operations; Hu et al. (2025b) developed a dispatching interval optimization model that simultaneously considers stochastic travel speed, uncertain passenger demand, and battery discharge fluctuations, revealing that the impact of stochasticity is more significant on passenger travel quality than on company operations. Nolz et al. (2022) addressed charging management at resource-constrained charging infrastructure by formulating it as a cumulative scheduling problem and solving it with constraint programming, integrating the charging schedule optimization within a template-based ALNS framework. Tang et al. (2025) found appropriate reservation ratios in mixed traffic systems reduce travel costs and congestion, though integration with spatial optimization remains unexplored.

2.2. Scheduling and control

Advanced scheduling shows significant potential. Jin and Xu (2021) established nodal multi-target characterization reducing action space dimensionality from $O(Nlog(n))$ to $O(N)$. Chung and Kwon (2015) extended flow-refueling location models to multi-period planning, highlighting computational challenges. Boyacłl et al. (2015) showed hierarchical decomposition achieves near-optimal solutions with computational savings.

In distributed computing, Ju et al. (2022) proposed ALADIN methods for hybrid microgrids, while Basso et al. (2021) achieved prediction errors below 6% using Bayesian machine learning. Our spatial optimization builds upon (Nourinejad et al., 2018)'s AV parking layout work, incorporating charging infrastructure constraints.

2.3. Optimization techniques and algorithms

Researchers have employed various optimization techniques for charging infrastructure. Mahyari and Freeman (2025) proposed approximate dynamic programming strategy for managing electric vehicle fleet charging at stations equipped with diverse multi-connector chargers, which can dynamically adapt to changing system conditions by learning from previous decisions and observations while handling uncertainties in vehicle arrival times, charging requirements, and dispatch schedules. Davatgari et al. (2024) develops a comprehensive Mixed-Integer Linear Programming model that simultaneously optimizes multiple critical decision dimensions of electric vehicle charging infrastructure. Through this comprehensive modeling approach, decision-makers can identify the optimal infrastructure configuration solution under given service level requirements. Tailored heuristic algorithms enhanced for specific scenarios have also been widely adopted (Zaidi et al., 2024; Qiu et al., 2026). Jordán et al. (2022) combined genetic algorithms with agent-based simulation, though without addressing multi-layered resource allocation.

For integrated systems, Dolgui et al. (2025) identify significant gaps between theoretical scheduling research and practical charging applications, particularly in capacitated and preemptive charging scenarios. Najafi et al. (2025), Amirteimoori et al. (2025) developed MILP models incorporating photovoltaic systems and battery storage, aligning with renewable integration work. Zhou et al. (2022b) highlighted that battery degradation costs can exceed daily charging costs, emphasizing optimization importance. Liu et al. (2024), Ma et al. (2025) demonstrated 37.35% cost reduction and 41.46% carbon emission reduction through data-driven optimization with solar integration. These algorithms all perform exceptionally well in specific resource optimization scenarios. However, the spatio-temporal dynamics of real-world parking facilities, and the corresponding trade-off between algorithmic efficiency and accuracy, remain a significant challenge.

2.4. Research gaps and our contribution

Critical gaps persist in existing approaches. First, integration deficiency-systems treat spatial, resource, and scheduling as separate problems. Unterluggauer et al. (2022) noted 'few papers embrace the combined problem to its full extent.' Second, limited scalability-algorithms target specific scales without flexibility. Third, single-objective focus-approaches optimize individual metrics rather than multiple objectives. Fourth, static optimization dominates, as Zhou et al. (2022a) noted, while dynamic adaptation remains rare. Fifth, theoretical-practical gaps persist with few real-world implementations.

Drawing on the scheduling mechanisms from Nejad et al. (2017), our framework further integrates spatial layout optimization. Our SAC-based module shares similarities with Chen et al. (2025)'s AL-SAC algorithm but extends it to hierarchical multi-layer coordination. The proposed three-layer optimization framework addresses these challenges through integrated optimization capturing interactions between spatial considerations, resource allocation, and scheduling dynamics, providing the first comprehensive solution to multi-dimensional EV charging management challenges (Table 1).

3. Three-Layer optimization framework for EV charging management

3.1. Problem definition and theoretical foundation

As shown in Fig. 2, this work introduces an innovative three-layer optimization framework addressing the multidimensional challenges in electric vehicle (EV) parking lot charging management. Traditional systems often treat spatial layout, resource allocation, and scheduling as isolated problems, resulting in suboptimal performance. Our approach leverages Hierarchical Decision Theory to achieve coordinated optimization through a structured yet interconnected strategy.

Fundamentally, our framework builds upon Bellman's Optimality Principle: if a policy π^* is optimal, then any sub-policy starting from state s_i following π^* is also optimal. The optimal value starting from state s_t can be formulated as:

$$V^{\pi^*}(s_t) = \max_{a_t} \left\{ R(s_t, a_t) + \gamma \mathbb{E}_{s_{t+1} \sim P(s_{t+1}|s_t, a_t)} \left[V^{\pi^*}(s_{t+1}) \right] \right\} \tag{1}$$

In reinforcement learning notation for EV charging optimization, π^* represents the optimal policy (decision-making strategy) that maximizes expected rewards, not an exponent of V. The system state s includes vehicle battery levels and charging station status, while actions a involve assignments of vehicles to stations and power allocation decisions. $R(s_t, a_t)$ denotes the multi-dimensional reward for taking action a_t in state s_t, balancing efficiency, movements, occupancy, waiting time, and costs. The discount factor γ determines how future rewards are valued compared to immediate ones. The expectation operator $\mathbb{E}$ accounts for the probabilistic nature of the system with uncertain vehicle arrivals and departures. These elements form the mathematical foundation for the Soft Actor-Critic approach used in the top scheduling layer of the framework.

We model the EV charging environment as a system Ω with capacity K, where vehicle arrivals follow a non-uniform Poisson process with time-varying arrival rate $\lambda(t)$. From a queuing perspective, the system follows a $G/G/C/K$ model, where G represents general (non-exponential) distributions for both arrival and service times, C represents charging stations and K represents maximum capacity. The complete system dynamics are captured by a Markov Decision Process (MDP) framework $\mathcal{M} = (S, \mathcal{A}, P, R, \gamma)$.
Key notation includes:

Parameter Set :

- $D \in \mathbb{Z}^+$ - Design demand (total EVs to be served)

Table 1
Summary of core models, methods, and objectives of charging management studies.

Reference	Model	Solution Method	Objective
(Amirteimoori et al., 2025)	Mixed Integer Linear Programming (MILP)	Parallel Optimal Algorithm (POAM)	Minimize infrastructure investment, operational costs, and delivery time.
(Basso et al., 2021)	EVRP with Chance-Constraints	Bayesian ML & Heuristic Optimization	Minimize expected energy consumption and variance under traffic uncertainty.
(Boyacłl et al., 2015)	Multi-objective MILP	GIS Preprocessing & Optimization Solver	Optimize operator profit, user satisfaction, and fleet size for car-sharing systems.
(Cao et al., 2018)	Mobility-aware Charging Decision	Periodical Reservation Updating	Minimize total trip duration under mobility uncertainty.
(Chen et al., 2025)	Constrained MDP (CMDP)	Augmented Lagrangian SAC (AL-SAC)	Minimize charging costs while ensuring battery lifespan and grid constraints.
(Chung and Kwon, 2015)	Multi-period Flow-refueling Model	Myopic & Optimization Methods	Maximize traffic flow coverage over multiple periods.
(Davatgari et al., 2024)	Location-Allocation for Fixed Routes	MIP	Minimize investment costs while meeting scheduling constraints.
(Habib et al., 2025)	Planning with ESS & Energy Mgmt.	Probabilistic Modeling & Optimization	Minimize total cost including investment and energy loss.
(Hu et al., 2025b)	Stochastic Dispatching Inverval optimization with chance constraints	Improved genetic algorithm based on probabilistic evolution model	Minimize passenger travel cost and company operation cost.
(Jin and Xu, 2021)	Stochastic Dynamic Programming	SAC + NMT Policy Characterization	Minimize costs under electricity price and renewable uncertainty.
(Jordán et al., 2022)	Agent-based Location Model	GA & Simulation	Optimize spatial placement for urban mobility efficiency.
(Ju et al., 2022)	Distributed Power Flow Model	Bi-level ALADIN Method	Ensure robust convergence in hybrid microgrids.
(Liu et al., 2024)	Energy Hub Model (PV + BES)	Data-driven Simulation	Maximize depot profit and reduce net grid load.
(Ma et al., 2025)	Stochastic Planning Model	Latin Hypercube Sampling	Minimize total lifecycle costs and carbon emissions.
(Mahyari and Freeman, 2025)	MDP	Approximate Dynamic Programming	Minimize fleet charging costs under uncertainty.
(Najafi et al., 2025)	Joint Infrastructure & Scheduling (MILP)	Benders Decomposition	Minimize total investment and operational costs under grid constraints.
(Nejad et al., 2017)	Online Scheduling and Pricing	VCG-based Mechanism Design	Maximize social welfare and ensure strategy-proofness in charging markets.
(Nolz et al., 2022)	Consistent EVRP with Backhauls	Template-based ALNS + CP	Optimize costs while maximizing driver and arrival time consistency.
(Nourinejad et al., 2018)	Parking Facility Layout (MINLP)	Benders Decomposition & Heuristics	Minimize vehicle relocations and maximize space efficiency.
(Qiu et al., 2026)	Robust MIP & stochastic programming & robust optimization	Hybrid heuristic algorithm & neighborhood search	Minimize total cost(vehicle, charging, trip fixed cost, lost time cost, and congestion cost.)
(Tang et al., 2025)	Bottleneck Model (DUE)	Analytical Derivation & Numerical Analysis	Manage congestion and parking constraints in mixed SAV/RV traffic.
(Xu et al., 2018)	Mobility-Charging Coupling Model	Big Data Analytics	Mitigate grid peak loads via personalized charging recommendations.
(Zaidi et al., 2024)	Preemptive Charging Scheduling	MILP & Iterated Local Search	Minimize required grid peak capacity while satisfying demands.
(Zhou et al., 2022a)	Total Social Cost Location Model	Genetic Algorithm	Minimize total social costs (investment, operation, user travel).

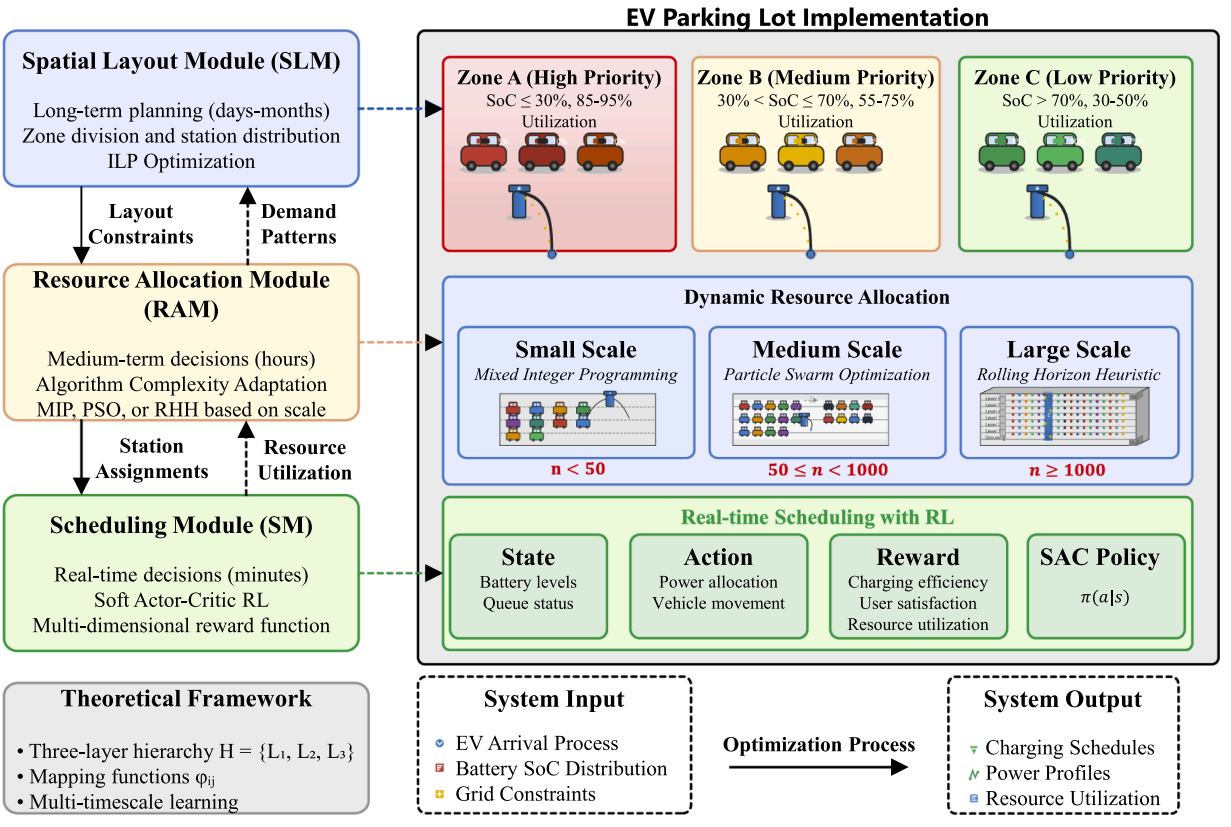

Fig. 2. Hierarchical approach of electric vehicle charging management with integrated information flows.

- $\lambda(t) : \mathbb{R}^+ \mapsto \mathbb{R}^+$ - Time-varying vehicle arrival rate function
- $\mu_v \sim \mathcal{F}_\mu$ - Parking time distribution for vehicle v
- $\mathbf{L} = (L, W) \in \mathbb{R}^2$ - Parking lot physical dimensions
- $\mathbf{C} = C_s, C_z, C_p$ - Capacity parameters (stations, zones, power)
- $\eta \in (0, 1]$ - Charging efficiency coefficient
- $\mathbf{p} = p_t | t \in \mathcal{T}$ - Time-varying electricity price vector
- $\mathbf{a} = (\alpha_1, \alpha_2, \ldots, \alpha_n)$ - Multi-objective weights
- $\mathcal{V} = v_1, v_2, \ldots, v_n$ - Electric vehicle set
- $\mathcal{STA} = sta_1, sta_2, \ldots, sta_m$ - Charging station set
- $\mathcal{T} = 0, \Delta t, 2\Delta t, \ldots, T$ - Discretized time periods
- $\mathcal{Z} = A, B, C$ - Functional zone set

Decision Variables Δ:

- $\mathbf{X} = x_{v,s,t} \in \{0, 1\} | v \in \mathcal{V}, s \in \mathcal{S}, t \in \mathcal{T}$ - Charging station assignment
- $\mathbf{Y} = y_{v,z} \in \{0, 1\} | v \in \mathcal{V}, z \in \mathcal{Z}$ - Zone assignment
- $\mathbf{PO} = PO_{v,t} \in [0, PO_{\max}] | v \in \mathcal{V}, t \in \mathcal{T}$ - Charging power allocation
- $\mathbf{E} = E_{v,t} \in [0, E_{\max}] | v \in \mathcal{V}, t \in \mathcal{T}$ - Battery energy state
- $\mathbf{M} = m_{v,t} \in \{0, 1\} | v \in \mathcal{V}, t \in \mathcal{T}$ - Vehicle movement operations

Fig. 3 illustrates a 120m × 180m electric vehicle parking lot with 2102 spaces organized into four functional zones (high priority Zone No.1, medium priority Zone No.2, low priority Zone No.3, and general parking Zone No.4) optimized for charging resource allocation based on vehicle battery state-of-charge, with detailed representations of vehicles and charging infrastructure demonstrating the spatial distribution strategy.

3.2. Multi-layer architecture and system integration

Our proposed framework systematically decomposes the intricate charging management system into a three-tiered intercorrelated architecture, where each layer operates over distinct time scales and decision horizons. This structural design is fundamentally

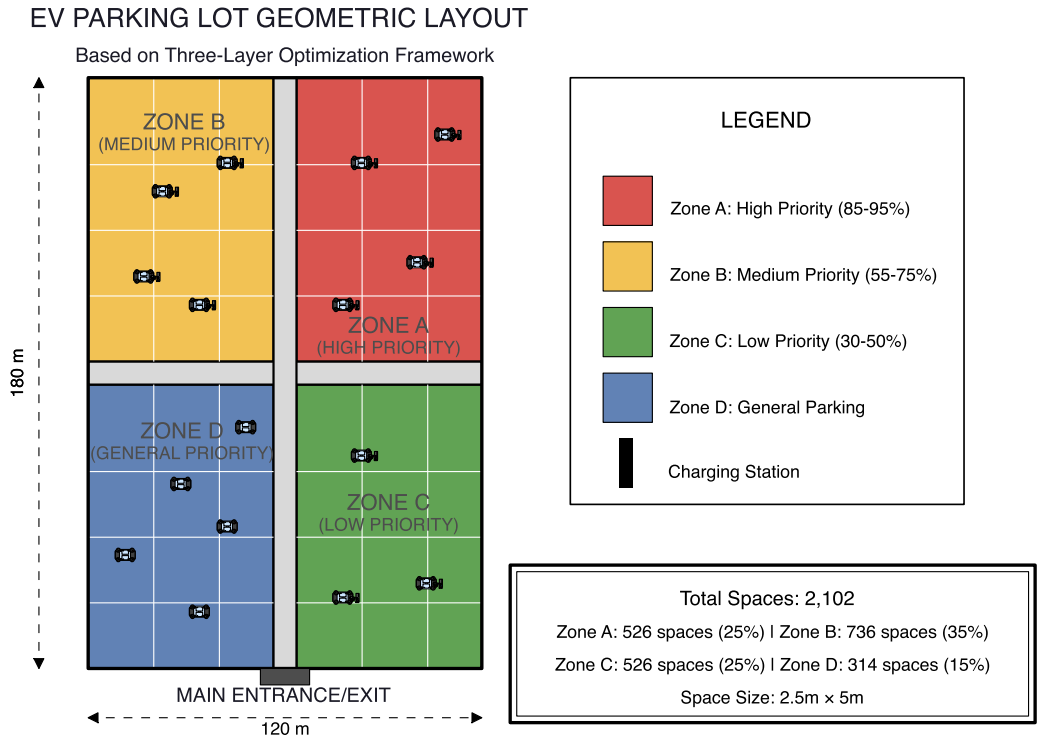

Fig. 3. Geometric layout of zoned EV parking lot based on three-Layer optimization framework.

rooted in multi-scale system theory, explicitly leveraging both a 'breadth-first' approach (layer-internal parallelization) and a 'depth-first' approach (layer-sequential optimization) to problem-solving. Formally, the system is structured as a three-layer hierarchy, $\mathcal{H} = \{L_1, L_2, L_3\}$. Inter-layer communication and interaction are realized through mapping functions $f_{i,j} : L_i \to L_j$ and feedback functions $g_{i,j} : L_i \to L_j$. Consequently, the entire architecture can be modeled as a Directed Acyclic Graph (DAG) $G = (Vertex, Edge)$, where vertices represent the layers and edges denote the directional information flows that guide the subsequent optimization process.

The overall management task is executed via a recursive equation system:

$$\begin{aligned} Y^* &= \arg\min_Y F_1(Y|\Theta) \\ X^* &= \arg\min_X F_2(X|\Theta, Y^*) \\ P^*, M^* &= \arg\min_{P,M} F_3(P, M|\Theta, Y^*, X^*) \end{aligned} \tag{2}$$

Here F_1, F_2, F_3 denote the objective functions for the respective layers.

Compared to traditional random charging resource distribution, our framework implements:

1. State-of-Charge Based Zoning Strategy (SBZS)
2. Dynamic Resource Allocation Mechanism (DRAM)

The parking lot is divided into three functional zones by solving:

$$\min_{A_z \in \mathcal{Z}} \left| \sum_{z \in \mathcal{Z}} A_z - (L \cdot W - A_{roadway}) \right|_2 + \varrho \sum_{z \in \mathcal{Z}} |A_z - A_z^{target}|_2 \tag{3}$$

where A_z is zone area and A_z^{target} is the target area based on capacity requirements, parameter ϱ balances these competing between these two objectives. First term: Ensures zones fill the available space; Second term: Tries to match target zone sizes;

The three primary system modules are:

1. Spatial Layout Module (SLM). Manages long-term planning decisions (days-months), optimizing parking configuration and charging station distribution.

SLM maximizes the availability index: $\phi_{\text{avail}} = \sum_{z \in \mathcal{Z}} \varphi_z \frac{C_z}{D_z}$ where C_z is zone capacity and D_z is predicted demand.

2. Resource Allocation Module (RAM). For our middle layer resource allocation module, we implement an adaptive algorithm selection strategy. While genetic algorithms have shown promise for certain charging infrastructure optimization problems (Zhou et al., 2022a)), our approach dynamically selects between MIP, PSO, and RHH based on problem scale to achieve optimal balance between solution quality and computational efficiency. Handles medium-term decisions (hours), implementing algorithm complexity adaptation strategy (ACAS) based on problem size $n = |\mathcal{V}| \times |\mathcal{STA}| \times |\mathcal{T}|$. The vehicle scale thresholds were empirically determined

by conducting preliminary experiments across the full range. Analysis of computational time growth rates and solution quality metrics revealed natural breakpoints where algorithm behavior transitioned significantly, leading to the identification of three operational regimes: small scale (≤ 50), medium scale (50 - 1000), and large scale (>1000).

- Small problems ($n \le n_1$): Mixed Integer Programming (MIP), $\mathcal{O}(2^n)$
- Medium problems ($n_1 < n \le n_2$): Particle Swarm Optimization (PSO), $\mathcal{O}(G \cdot P \cdot n)$
- Large problems ($n > n_2$): Rolling Horizon Heuristic (RHH), $\mathcal{O}(H \cdot n_{sub})$

3. Scheduling Module (SM). Manages real-time decisions (minutes), using Soft Actor-Critic Reinforcement Learning method to iteratively solve:

$$Q(s,a) = R(s,a) + \gamma \mathbb{E}_{s' \sim P(\cdot|s,a)} \left[\max_{a'} Q(s',a') \right]$$

In the reinforcement learning equations for EV charging optimization, $Q(s,a)$ represents the state-action value function that calculates expected cumulative rewards when taking action a in state s, with superscript s potentially indicating specific environmental conditions. $R(s,a)$ denotes the immediate reward obtained from this state-action pair. The discount factor γ (between 0 and 1) balances immediate versus future rewards. $\mathbb{E}_{s' \sim P(\cdot|s,a)}$ is the expectation operator over the next state s', sampled according to transition probability $P(\cdot|s,a)$. Finally, $\max_{a'} Q(s',a')$ represents the maximum Q-value obtained by selecting the optimal action a' in the next state s'. These elements collectively form the mathematical foundation for the decision-making process in the scheduling module of the three-layer optimization framework.

Our framework achieves both vertical integration (between layers) and horizontal coordination (within layers). Vertical integration uses state mapping function $\Phi : S_i \to S_{i+1}$ and decision mapping function $\Psi : \mathcal{A}_{i+1} \to \mathcal{A}_i$, while horizontal coordination ensures consistent decision variables through synchronized optimization.

3.3. Spatial layout optimization

The SLM optimizes the physical structure of the parking lot using Zonal Integer Programming Method (ZIPM). The layout problem is formulated as a combinatorial optimization with state space $Slayout$ having dimension $\dim(\text{ Slayout }) = 2^{L \times W/(l \times w)}$.

To make this tractable, we employ zone division based on the Compactness Principle and evaluate allocation stability using Nash Equilibrium concepts. An allocation is stable when: $\forall v \in \mathcal{V}, \forall z, z' \in \mathcal{Z} : U_v(z) \ge U_v(z')$ at $Y_{v,z} = 1$.

For all vehicles v and all zones z and z', when vehicle v is assigned to zone z (i.e., $Y_{v,z} = 1$), the utility of vehicle v in zone z must be greater than or equal to its utility in any other zone z'.

Components explanation:

- $\forall v \in V$: For each vehicle in the set of vehicles V
- $\forall z, z' \in Z$: For any zones in the set of zones Z
- $U_v(z) \ge U_v(z')$: The utility of vehicle v in zone z is not less than its utility in zone z'
- when $Y_{v,z} = 1$: The condition applies when vehicle v is assigned to zone z (decision variable $Y_{v,z} = 1$)

The zone boundary optimization problem is formulated as:

$$\min_{Y,\mathbf{B}} \sum_{v \in \mathcal{V}} \sum_{z \in \mathcal{Z}} c_{v,z} \cdot y_{v,z} + \beta \sum_{z \in \mathcal{Z}} \sum_{z' \in \mathcal{Z} : z' \ne z} \|\mathbf{b}_z - \mathbf{b}_{z'}\|_2$$

Subject to:

$$\begin{aligned}
\textstyle\sum_{z \in \mathcal{Z}} y_{v,z} &= 1, \quad \forall v \in \mathcal{V} \\
\textstyle\sum_{v, \mathcal{V}} y_{v,z} &\le C_z, \quad \forall z \in \mathcal{Z} \\
\text{Area}(z) = f(\mathbf{b}_z) &\le Area^z_{\max}, \quad \forall z \in \mathcal{Z} \\
\text{perimeter}(z) = g(\mathbf{b}_z) &\le Perimeter^z_{\max}, \quad \forall z \in \mathcal{Z} \\
\text{connectivity}(z) = h(\mathbf{b}_z) &= 1, \quad \forall z \in \mathcal{Z} \\
y_{v,z} &\le M \cdot \mathbb{I}\left(SoC_v \in \left[SoC^z_{\min}, SoC^z_{\max}\right]\right), \quad \forall v \in \mathcal{V}, \forall z \in \mathcal{Z}
\end{aligned} \tag{4}$$

The zones are defined by battery state ranges:

$$\begin{aligned}
\left[SoC^A_{\min}, SoC^A_{max}\right] &= [0.85, 0.95] \\
\left[SoC^B_{\min}, SoC^B_{max}\right] &= [0.55, 0.75] \\
\left[SoC^C_{\min}, SoC^C_{max}\right] &= [0.30, 0.50]
\end{aligned}$$

We optimize zone geometry using Voronoi diagrams. Given seed points $SP = sp_1, sp_2, \ldots, sp_{|\mathcal{Z}|}$, the Voronoi cell for zone z is:

$$V_z = \{x \in \mathbb{R}^2 \mid \|x - sp_z\|_2 \le \|x - sp_{z'}\|_2, \forall z' \ne z\} \tag{5}$$

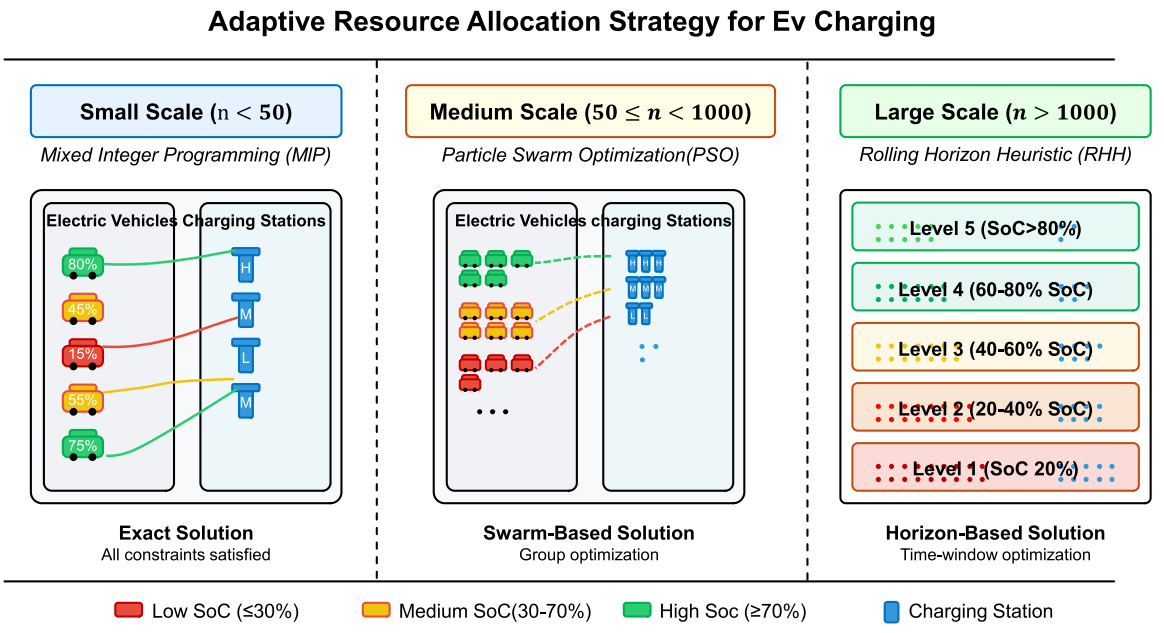

Fig. 4. Scale-adaptive resource allocation framework for electric vehicle charging systems.

We discretize the parking lot into a grid $G = \{g_{i,j} | 1 \le i \le N_x, 1 \le j \le N_y\}$ with $N_x = L/\Delta x$ and $N_y = W/\Delta y$. Assignment probability uses Softmax:

$$P(g_{i,j} \in z) = \frac{\exp(-\|x_{i,j} - sp_z\|_2/\tau)}{\sum_{z' \in Z} \exp(-\|x_{i,j} - sp_{z'}\|_2/\tau)} \tag{6}$$

After determining optimal zones, we optimize charging station distribution by solving:

$$\min_{\mathbf{locs} \in \mathcal{STA}} \sum_{z \in \mathcal{Z}} \left| \frac{|STA_z|}{|STA|} - \frac{C_z}{D} \right| + \lambda_{cs} \sum_{sta \in \mathcal{STA}} \sum_{sta' \in \mathcal{STA}, sta' \neq sta} \psi(\|\mathbf{locs} - \mathbf{locs}'\|_2) \tag{7}$$

3.4. Adaptive resource allocation strategy

The RAM assigns charging stations to vehicles across time periods while considering grid constraints, user demands, and system efficiency. The resource allocation problem has state space size $|S_{\text{resource}}| = (|S|+1)^{|V|\times|T|}$. The core problem is formulated as a Multi-constrained Bipartite Matching Problem with bipartite graph $BG = (VertexSet_1 \cup VertexSet_2, Edges)$, where $VertexSet_1 = V \times T$ and $VertexSet_2 = S \times T$.

As shown in Fig. 4, algorithm selection depends on facility scale: Mixed Integer Programming for small-scale, Particle Swarm Optimization for medium-scale, and Rolling Horizon Heuristic for large-scale EV charging environments.

3.4.1. Mixed integer programming (MIP) for small size case

For small-scale charging facilities with $n \le n_1$ vehicles, where n_1 represents the computational tractability threshold (typically 50 vehicles), we formulate the resource allocation problem as a MIP model. This formulation guarantees global optimality while maintaining computational feasibility for limited problem sizes ($n \le n_1$). The objective function minimizes the total system cost comprising electricity consumption costs and vehicle relocation costs:

$$\min_{X,P} \sum_{v \in V} \sum_{t \in T} \sum_{sta \in STA} (\alpha_1 \cdot p_{v,t} \cdot PO_{v,t} \cdot x_{v,sta,t} \cdot \Delta t + \alpha_2 \cdot c_{v,sta,t} \cdot x_{v,sta,t}) \tag{8}$$

where $\mathcal{V}$, $\mathcal{T}$, and $\mathcal{S}$ denote the sets of vehicles, time periods, and charging stations, respectively; $x_{v,s,t} \in \{0,1\}$ is a binary decision variable indicating whether vehicle v is assigned to charging station s at time t; $PO_{v,t} \in \mathbb{R}_+$ represents the charging power allocated to vehicle v at time t; p_t denotes the time-varying electricity price at period t; $c_{v,s,t}$ represents the relocation cost for vehicle v to access station s at time t; α_1 and α_2 are weighting coefficients for electricity and relocation costs, α_1 scales the importance of minimizing electricity consumption costs. α_2 weights the operational cost associated with vehicle movements between parking spots and charging stations; Δt is the discrete time interval.

The optimization is subject to the following constraints:

Vehicle Assignment Constraints:

$$\sum_{s\in S} x_{v,sta,t} \le 1, \quad \forall v \in \mathcal{V}, \forall t \in \mathcal{T} \tag{9}$$

Constraint Eq. (9) ensures that each vehicle can be assigned to at most one charging station at any given time period.

Charging Station Capacity Constraints:

$$\sum_{v\in\mathcal{V}} x_{v,sta,t} \le 1, \quad \forall s \in \mathcal{S}, \forall t \in \mathcal{T} \tag{10}$$

Constraint Eq. (10) enforces that each charging station can serve at most one vehicle simultaneously.

Grid Power Constraints:

$$\sum_{v\in\mathcal{V}} \sum_{s\in\mathcal{S}} PO_{v,t} \cdot x_{v,sta,t} \le PO_{gmax}, \quad \forall t \in \mathcal{T} \tag{11}$$

where PO_{gmax} represents the maximum power capacity available from the grid. Constraint Eq. (11) ensures that the aggregate power demand does not exceed grid capacity limits.

Charging Power Bounds:

$$PO_{v,t} \le PO_{\max} \cdot \sum_{sta\in\mathcal{STA}} x_{v,sta,t}, \quad \forall v \in \mathcal{V}, \forall t \in \mathcal{T} \tag{12}$$

$$PO_{v,t} \ge PO_{\min} \cdot \sum_{sta\in\mathcal{STA}} x_{v,sta,t}, \quad \forall v \in \mathcal{V}, \forall t \in \mathcal{T} \tag{13}$$

Constraints Eq. (12) and Eq. (13) establish the operational bounds on charging power, where $P_{\max}$ and $P_{\min}$ denote the maximum and minimum allowable charging rates, respectively. These constraints ensure that charging power is within feasible limits only when a vehicle is connected to a station.

Battery State Evolution:

$$E_{v,t} = E_{v,t-1} + \eta \cdot PO_{v,t} \cdot \Delta t - E_{v,t}^{\text{self}}, \quad \forall v \in \mathcal{V}, \forall t \in \mathcal{T} \tag{14}$$

where $E_{v,t}$ represents the battery energy level of vehicle v at time t, $\eta \in (0, 1]$ is the charging efficiency coefficient, and $E_{v,t}^{\text{self}}$ accounts for self-discharge losses. **Battery Capacity Constraints:**

$$E_{v,t} \le E_{\max}, \quad \forall v \in \mathcal{V}, \forall t \in \mathcal{T} \tag{15}$$

User Satisfaction Constraints:

$$E_{v,T_v^{\text{dep}}} \ge E_v^{\text{req}}, \quad \forall v \in \mathcal{V} \tag{16}$$

where T_v^{dep} denotes the departure time of vehicle v and E_v^{req} represents the minimum required energy level specified by the user.

Zone Assignment Constraints:

$$\sum_{sta\in\mathcal{STA}_z} x_{v,s,t} \le M \cdot y_{v,z}, \quad \forall v \in \mathcal{V}, \forall z \in \mathcal{Z}, \forall t \in \mathcal{T} \tag{17}$$

where $\mathcal{STA}_z \subseteq \mathcal{STA}$ denotes the subset of charging stations in zone z, $y_{v,z} \in \{0, 1\}$ indicates whether vehicle v is assigned to zone z, and M is a sufficiently large constant. This constraint ensures consistency between zone assignments and charging station allocations.

3.4.2. Particle swarm optimization (PSO) for medium problems

For medium-scale charging facilities where $n_1 < n \le n_2$ (typically 50–500 vehicles), we employ a PSO metaheuristic. This bio-inspired algorithm offers an effective balance between solution quality and computational efficiency, achieving near-optimal solutions with polynomial time complexity. Each particle represents a potential allocation solution with position and velocity vectors updated by:

$$V_i^{(k+1)} = \omega V_i^{(k)} + c_1 r_1(\mathbf{pbest}_i - \mathbf{X}_i^{(k)}) + c_2 r_2(\mathbf{gbest} - \mathbf{X}_i^{(k)}) \tag{18}$$

$$\mathbf{X}_i^{(k+1)} = \mathbf{X}_i^{(k)} + V_i^{(k+1)} \tag{19}$$

where ω is the time-varying inertia weight controlling exploration-exploitation balance; *pbest* represents the personal best position discovered by particle i throughout its search history, and *gbest* denotes the global best position identified across the entire swarm population; $c_1, c_2 \in \mathbb{R}_+$ are cognitive and social acceleration coefficients, respectively; r_1, r_2 are uniformly distributed random numbers generated independently for each dimension at every iteration.

Since the resource allocation problem involves binary decision variables $x_{v,s,t} \in \{0, 1\}$, we employ a sigmoid transformation to map continuous position values to discrete assignments. The probability of assigning vehicle v to station s at time t is given by:

$$P(x_{v,s,t} = 1) = \frac{1}{1 + \exp(-\tau \cdot x_{v,s,t}^{(i)})} \tag{20}$$

Table 2
Comparison of optimization algorithms for resource allocation.

Algorithm	Computational Complexity	Solution Quality	Vehicle Scale	Memory Requirements	Convergence Properties
MIP	$O(2^n)$	Optimal	Small (≤50)	High	Guaranteed
PSO	$O(n^2)$	Near-optimal (95-98%)	Medium (50–500)	Medium	Probabilistic
RHH	$O(n \log n)$	Good (90-95%)	Large (>500)	Low	Fast

where $x_{v,s,t}^{(i)}$ is the continuous position value for particle i, and $\tau > 0$ is a temperature parameter controlling the stochasticity of the mapping. The discrete assignment is then determined stochastically:

$$x_{v,s,t} = \begin{cases} 1, & \text{if } U(0,1) < P(x_{v,s,t} = 1) \\ 0, & \text{otherwise} \end{cases} \tag{21}$$

3.4.3. Rolling horizon heuristic for large problems

For large-scale charging facilities where $n > n_2$ (typically exceeding 500 vehicles), the computational burden of exact or metaheuristic approaches becomes prohibitive for real-time applications. We therefore develop a Rolling Horizon Heuristic (RHH) that decomposes the temporal optimization problem into a sequence of tractable subproblems while maintaining theoretical performance guarantees.

The rolling horizon approach is grounded in the principle of temporal decomposition, where the full planning horizon $\mathcal{T}$ is partitioned into overlapping windows of length H. At each decision epoch t, the algorithm solves a restricted optimization problem over the horizon $[t, t+H]$, implements only the immediate decisions, and then advances to the next epoch. This methodology balances computational tractability with solution quality by exploiting the diminishing importance of future decisions in dynamic environments.

Let $\mathcal{T}_t^H = \{t, t+1, \ldots, \min(t+H-1, T)\}$ denote the planning window at time t. The RHH solves the following restricted optimization problem at each decision epoch:

$$\min_{X_t, PO_t} \sum_{v \in \mathcal{V}_t} \sum_{\tau=t}^{t+H} \sum_{sta \in \mathcal{STA}_{v,\tau}} (PO_{v,\tau}) \cdot x_{v,sta,\tau} \tag{22}$$

where $\mathcal{V}_t$ represents the set of vehicles present at time t, and $\mathcal{STA}_{v,\tau}^c \subseteq \mathcal{STA}$ denotes a restricted set of candidate charging stations for vehicle v at time τ. The candidate set is constructed based on spatial proximity and availability criteria:

$$\mathcal{STA}_{v,\tau}^c = \{sta \in \mathcal{STA} : d_{v,sta} \le d_{\max} \text{ and availability}(sta, \tau) = 1\} \tag{23}$$

Despite the myopic nature of rolling horizon optimization, we establish theoretical bounds on solution quality. Let J^* denote the optimal value of the full problem and J_{RHH} the value obtained by RHH. The approximation ratio is bounded by:

$$\rho_{RHH} = \frac{J_{RHH}}{J^*} \le 1 + \frac{\gamma}{1-\gamma} \cdot \frac{\max_{v,sta,t} c_{v,sta,t}}{\min_{v,sta,t} c_{v,sta,t}} \tag{24}$$

where $\gamma \in (0,1)$ is the effective discount factor over the horizon length H. To balance grid load, we incorporate Peak-Valley Difference Minimization Strategy:

$$\min_{X,PO} \alpha_1 \cdot \sum_{v \in \mathcal{V}} \sum_{sta \in \mathcal{STA}} \sum_{t \in \mathcal{T}} p_t \cdot PO_{v,sta} \cdot x_{v,sta,t} \cdot \Delta t + \alpha_2 \cdot |\max_{sta \in \mathcal{STA}} PO_s^{grid} - \min_{s \in S} PO_s^{grid}| + \alpha_3 \cdot \sum_{t \in \mathcal{T}} (PO_t^{grid} - \bar{PO})^2 \tag{25}$$

We employ Lagrangian Relaxation for efficiency:

$$L(\mathbf{X}, \mathbf{PO}, \lambda) = \sum_{v \in V} \sum_{t \in T} \sum_{sta \in STA} c_{v,sta,t}(PO_{v,t}) \cdot x_{v,sta,t} + \sum_{t \in T} \lambda_t \left(\sum_{v \in V} \sum_{sta \in STA} PO_{v,t} \cdot x_{v,sta,t} - PO_g \right) \tag{26}$$

The dual problem is: $\max_{\lambda \ge 0} \min_{\mathbf{X},\mathbf{P}} L(\mathbf{X}, \mathbf{P}, \lambda)$

Table. 2 provides a comparative analysis of the three algorithms employed in the resource allocation layer of our framework. The algorithms exhibit distinct characteristics across five key dimensions. MIP delivers optimal solutions but is computationally tractable only for small-scale problems with fewer than 50 vehicles. PSO strikes a balance between solution quality and computational efficiency, making it suitable for medium-scale facilities handling 50–500 vehicles, with solution quality typically within 2–5% of the global optimum. For large-scale operations exceeding 500 vehicles, RHH provides good solutions with significantly reduced computational requirements, achieving approximately 90–95% of optimal performance. These results demonstrate the effectiveness of our adaptive algorithm selection strategy in balancing solution quality with computational tractability across varying facility scales.

3.5. Reinforcement learning-based real-time scheduling

The SM employs Soft Actor-Critic (SAC) deep reinforcement learning to learn optimal scheduling policies. Recent work by (Chen et al., 2025) demonstrated that combining SAC with the augmented Lagrangian method (AL-SAC) can effectively handle constraints

while maintaining high solution optimality, which inspired our multi-dimensional reward function design. The scheduling MDP is formalized as,

$$\mathcal{MDP}_{schedule} = (S_{schedule}, A_{schedule}, P_{schedule}, R_{schedule}, f) \tag{27}$$

State Space:

$$S_{schedule} = s_t = (v_t, cs_t, env_t) \mid t \in \mathcal{T} \tag{28}$$

where $\mathbf{v}_t$ represents the vehicle state vector, encompassing spatial position, battery state-of-charge, and temporal constraints including arrival and departure times; $\mathbf{cs}_t$ denotes the charging station state vector, capturing occupancy status and operational availability; and $\mathbf{env}_t$ represents the environmental state vector, incorporating time-varying electricity prices, grid load conditions, and temporal factors that influence system dynamics. **Action Space**:

$$A_{schedule} = a_t = (P_t, X_t, M_t) \mid t \in \mathcal{T} \tag{29}$$

where $\mathbf{PO}_t$ denotes charging power allocation matrix; $\mathbf{X}_t$ denotes charging station assignment matrix, and $\mathbf{M}_t$ denotes vehicle relocation operation matrix. **State Transitions**:

$$P_{schedule}(s_{t+1} \mid s_t, a_t) = P_{veh}(v_{t+1} \mid v_t, a_t) \cdot P_{cs}(cs_{t+1} \mid cs_t, a_t) \cdot P_{env}(env_{t+1} \mid env_t, a_t) \tag{30}$$

The state transition probability $P(\mathbf{s}_{t+1}|\mathbf{s}_t, \mathbf{a}_t)$ can be factorized into three conditionally independent components: the vehicle state transition $P_v(\mathbf{v}_{t+1}|\mathbf{v}_t, \mathbf{a}_t)$ capturing battery dynamics and vehicle movements, the charging station transition $P_{cs}(\mathbf{cs}_{t+1}|\mathbf{cs}_t, \mathbf{a}_t)$ modeling occupancy changes, and the environmental transition $P_{env}(\mathbf{env}_{t+1}|\mathbf{env}_t)$ representing exogenous factors such as electricity prices and grid conditions. **Battery dynamics**:

$$E_{v,t+1} = E_{v,t} + \eta \cdot P_{v,t} \cdot \Delta t - E^{self}_{v,t} + \delta_{arrival}(v,t) \cdot E^{init}_{v} - \delta_{departure}(v,t) \cdot E_{v,t} \tag{31}$$

Reward Function:

$$R_{schedule}(s_t, a_t, s_{t+1}) = \sum w_i \cdot R_i(s_t, a_t, s_{t+1}) \tag{32}$$

With components:

1. **Charging cost**: $R_1 = -\sum_{v\in\mathcal{V}} p_t \cdot P_{v,t} \cdot \Delta t$
2. **User satisfaction**: $R_2 = \sum_{v\in\mathcal{V}} f(E_{v,t}, E^{req}_{v,t}, T^{dep}_{v})$
3. **Movement penalties**: $R_3 = -\sum_{v\in\mathcal{V}} [c_{fix} \cdot \mathbb{I}(m_{v,t} = 1) + c_{var} \cdot d_{v,t}]$
4. **Resource utilization**: $R_4 = \phi\left(\frac{\sum_{v\in\mathcal{V}} \sum_{s\in\mathcal{S}_{v,s,t}}}{|S|}\right)$
5. **Load balancing**: $R_5 = -\text{var}(P_{i,t} \mid v \in \mathcal{V}_t)$
6. **SAC maximizes entropy-enhanced rewards**:

$$\pi^* = \arg\max_{\pi} \mathbb{E}_{\pi\sim\tau}\left[\sum_{t=0}^{\infty} \gamma^t (R_{schedule}(s_t, a_t, s_{t+1}) + \alpha\mathcal{H}(\pi(\cdot|s_t)))\right]$$

The algorithm uses Soft Actor-Critic (SAC) networks to approximate the value functions, following the approach proposed by (Chen et al., 2025).

3.6. Hierarchical integration and performance-based coordination

The framework's key strength lies in its performance-based coordination mechanisms between layers, which enable effective integration without requiring differentiability of the optimization algorithms. We design an Inter-layer Information Flow Graph (IIFG) that facilitates bidirectional communication through structured performance metrics and operational indicators.

3.6.1. Vertical integration through performance feedback

The vertical integration occurs through two complementary mechanisms: forward constraint propagation and performance-based feedback loops.

1. Forward Constraint Propagation (SLM → RAM → SM):

The forward flow establishes operational boundaries for each subsequent layer:

$$\text{Layout} \rightarrow \text{Allocation}: \quad \Phi_{1,2}(Y, B) = (\mathcal{V}_z, \mathcal{STA}_z, \text{Area}_z), \quad z \in \mathcal{Z} \tag{33}$$

$$\text{Allocation} \rightarrow \text{Scheduling}: \quad \Phi_{2,3} = \{X_{v,sta,t} \mid v \in \mathcal{V}, sta \in \mathcal{STA}, t \in \mathcal{T}\} \tag{34}$$

2. Performance Feedback Loop (SM → RAM → SLM):

Instead of gradient-based updates, the framework employs performance metrics to guide upper-layer adjustments:

$$\text{Scheduling} \rightarrow \text{Allocation}: \quad \Psi_{3,2}(PO, M) = \{u_{v,sta,t}, VI_{sta,t}, \rho_{sta,t}\} \tag{35}$$

$$\text{Allocation} \rightarrow \text{Layout}: \quad \Psi_{2,1}(X^*) = \{CI_z, UR_z, RR_z\} \tag{36}$$

where $u_{v,sta,t}$ represents utilization rates, $VI_{sta,t}$ denotes violation indicators, $\rho_{sta,t}$ captures performance scores, CI_z indicates zone congestion indices, UR_z represents zone utilization ratios, and RR_z denotes reallocation requests.

3.6.2. Performance-Based coordination protocol

The horizontal coordination within each layer employs synchronized optimization based on shared performance objectives. For the resource allocation layer, charging station assignments X and power allocation PO are jointly optimized using an Alternating Direction Method of Multipliers (ADMM) approach:

$$X^{k+1} = \arg\min_{X} \mathcal{L}_{\rho}(X, PO^{k}, \lambda^{k}) \tag{37}$$

$$PO^{k+1} = \arg\min_{PO} \mathcal{L}_{\rho}(X^{k+1}, PO^{k}, \lambda^{k}) \tag{38}$$

$$\lambda^{k+1} = \lambda^{k} + \rho(A \cdot X^{k+1} + B \cdot PO^{k+1} - c) \tag{39}$$

3.6.3. Multi-timescale adaptive mechanism

The framework implements multi-timescale learning with update cycles varying by layer to balance responsiveness with computational efficiency:

$$\tau_{\text{SLM}} = \kappa_{1,2} \cdot \tau_{\text{RAM}} = \kappa_{1,3} \cdot \tau_{\text{SM}} \tag{40}$$

$$\tau_{\text{RAM}} = \kappa_{2,3} \cdot \tau_{\text{SM}} \tag{41}$$

where τ_{SLM}, τ_{RAM}, and τ_{SM} represent the update periods for spatial layout (days to weeks), resource allocation (hours), and scheduling (minutes) modules respectively. The scaling factors $\kappa_{i,j}$ ensure temporal consistency across the multi-scale framework.

3.6.4. Hierarchical adaptive optimization process

The overall optimization process follows a Hierarchical Adaptive Optimization (HAO) protocol that responds to performance feedback:

1. Forward Optimization Phase:

1. **Optimize SLM:** $\arg\min F_1(Y, B)$ subject to physical constraints
2. **Pass constraints:** $\Phi_{1,2}(Y, B)$ defines operational boundaries for RAM
3. **Optimize RAM:** $\arg\min F_2(X|\Phi_{1,2})$ within spatial constraints
4. **Pass assignments:** $\Phi_{2,3}(X^*)$ provides scheduling constraints
5. **Optimize SM:** $\arg\min F_3(P, M|\Phi_{2,3})$ for real-time operations

2. Performance Evaluation and Adaptive Response:

1. **Monitor performance:** Collect metrics $\Psi_{2,3}(P, M)$ from operational layer
2. **Trigger RAM adaptation:** If $CI_z > CI_{threshold}$ or $VI_{sta,t} > VI_{max}$:
   - Adjust allocation priorities based on congestion patterns
   - Rebalance vehicle-station assignments using performance scores
3. **Aggregate zone metrics:** Compute $\Psi_{2,1}(X^*)$ from allocation performance
4. **Trigger SLM reconfiguration:** If $UR_z < UR_{\min}$ or systematic congestion detected:
   - Initiate zone boundary adjustment based on utilization patterns
   - Redistribute charging stations according to demand concentration

This adaptive mechanism ensures that each layer responds to actual operational conditions rather than relying on theoretical gradient information that may not be computable in discrete optimization contexts. The performance thresholds ($CI_{threshold}$, $VI_{\max}$, $UR_{\min}$) are calibrated through empirical testing to balance system stability with responsiveness to changing conditions.

3.6.5. Coordination stability analysis

The stability of the coordination mechanism is ensured through bounded performance metrics and controlled update frequencies. Let $\mathcal{P}^{(k)}$ represent the system performance at iteration k. The framework achieves coordination stability when:

$$\|\mathcal{P}^{(k+1)} - \mathcal{P}^{(k)}\| \leq \epsilon_{perf} \tag{42}$$

where ϵ_{perf} is the performance convergence threshold. The multi-timescale update strategy prevents oscillations by ensuring that faster layers reach quasi-steady state before slower layers adapt:

$$\frac{\tau_{\text{SM}}}{\tau_{\text{RAM}}} < \delta_1 \quad \text{and} \quad \frac{\tau_{\text{RAM}}}{\tau_{\text{SLM}}} < \delta_2 \tag{43}$$

where δ_1 and δ_2 are stability margins determined through empirical analysis. This temporal hierarchy ensures that real-time decisions adapt within constraints imposed by strategic planning while maintaining overall system coherence.

Experiments demonstrate that this performance-based coordination approach significantly outperforms both single-layer optimization and non-coordinated multi-layer methods, particularly in dynamic environments with demand fluctuations, price changes, and equipment failures. The absence of gradient requirements makes the framework robust to the discrete nature of many decision variables while maintaining effective inter-layer communication.

3.7. Theoretical performance and computational analysis

Our three-layer framework provides theoretical performance guarantees and manageable computational complexity.

Convergence Analysis: If each layer's optimization problem satisfies regularity conditions, the framework converges to at least a local optimum. The convergence rate follows:

$$\|\mathbf{z}^k - \mathbf{z}^*\|_2 \leq (1-\rho)^k \|\mathbf{z} - \mathbf{z}^*\|_2$$

Where $\mathbf{z}$ represents all decision variables and $\rho \in (0,1)$ is the convergence coefficient.

Stability Analysis: The framework demonstrates robustness to parameter perturbations. Each layer's condition number $\kappa_i = \lambda_{\max}(\nabla^2 F_i)/\lambda_{\min}(\nabla^2 F_i)$ affects sensitivity to disturbances. We employ regularization techniques to control these condition numbers.

Approximation Ratio: The framework achieves near-optimal solutions with approximation error bounded by: $F(\mathbf{z}^*)/F(\mathbf{z}_{OPT}) \leq 1+\varepsilon$

Empirical testing shows ε typically within 5%, meaning our approach achieves at least 95% of global optimality.

Computational Complexity: The total complexity combines:

$$T_{total} = T_{SLM} + T_{RAM} + T_{SM} + T_{interaction} \tag{44}$$

Where:

$T_{SLM} = O(2^{|\mathcal{Z}|\cdot N_x \cdot N_y})$ (reduced to polynomial time with heuristics)

T_{RAM} varies by algorithm choice

$T_{SM} = O(|\mathcal{V}| \cdot |\mathcal{S}| \cdot |\mathcal{T}| \cdot N_{iter})$

$T_{interaction} = O(|\mathcal{V}| \cdot |\mathcal{Z}| \cdot |\mathcal{S}| \cdot |\mathcal{T}|)$

4. Solution methodology and implementation

4.1. Spatial layout module implementation

The Spatial Layout Module (SLM) translates the theoretical Zonal Integer Programming Method defined in Section 3.3 into a tractable computational workflow. We implement this through a two-stage optimization approach that balances initialization speed with solution precision.

Stage 1: Iterative Initialization. The first stage establishes a stable initial configuration to reduce the search space for the subsequent integer programming model. Utilizing the Voronoi formulation from Eq. (5), the system executes an iterative centroid update process. Unlike the theoretical definition, the practical implementation defines strict convergence criteria: the iteration terminates only when the Euclidean displacement of seed points between consecutive steps satisfies $\|\mathbf{sp}_z^{(k+1)} - \mathbf{sp}_z^{(k)}\| < \varepsilon$, where ε is a pre-defined tolerance threshold.

Stage 2: Exact Boundary Optimization. Once initialized, the zone boundary optimization problem Eq. (4) is solved to exactness. To handle the combinatorial complexity of the state space, we employ the Gurobi Optimizer, a commercial mathematical programming solver. The implementation leverages Gurobi's advanced branch-and-bound algorithms augmented with cutting plane methods.

4.2. Resource allocation module implementation

The Resource Allocation Module (RAM) implements an adaptive algorithm selection mechanism based on problem scale $n = |\mathcal{V}| \times |\mathcal{STA}| \times |\mathcal{T}|$, ensuring computational tractability across varying facility sizes. For small-scale problems where $n < 50$, we employ exact mixed-integer programming (MIP) formulation. The MIP solver formulates the objective function as specified in Eq. (3.4.1), incorporating all constraints defined in Eq. (9) through Eq. (17). The branch-and-cut algorithm systematically explores the solution space, providing globally optimal assignments X^* and power allocations P^*.

For medium-scale problems where $50 \leq n < 1000$, the framework employs Particle Swarm Optimization (PSO) to balance solution quality with computational efficiency. The PSO implementation initializes a swarm of N_p particles, each representing a potential solution in the continuous relaxation of the assignment space. During each iteration, particle velocities are updated according to $v_i = w \cdot v_i + c_1 \cdot r_1 \cdot (pbest_i - x_i) + c_2 \cdot r_2 \cdot (gbest - x_i)$, where w represents the inertia weight, c_1 and c_2 are cognitive and social acceleration coefficients, and r_1, r_2 are uniformly distributed random numbers. The positions are subsequently updated as $x_i = x_i + v_i$, with sigmoid transformation applied to handle discrete decision variables. The inertia weight follows a linear decay schedule: $w = w_{\max} - (w_{\max} - w_{\min}) \cdot (\text{iter}/\text{max\_iter})$, promoting exploration in early iterations and exploitation in later stages.

Large-scale problems with $n \geq 1000$ necessitate the Rolling Horizon Heuristic (RHH) approach to maintain real-time performance. The RHH decomposes the temporal optimization problem into a sequence of smaller, tractable subproblems. At each time step t,

the algorithm defines a planning horizon $\mathcal{T}_H = [t, \min(t + H - 1, T)]$ and identifies the set of active vehicles $\mathcal{V}_t = \{v \in \mathcal{V} : t^v_{\text{arrival}} \leq t \leq t^v_{\text{departure}}\}$. To further reduce computational complexity, candidate charging stations for each vehicle are restricted based on spatial proximity, creating a reduced search space. The algorithm then solves the restricted optimization problem over the planning horizon using a greedy assignment strategy that prioritizes vehicles with lower battery states and assigns them to the nearest available high-power charging stations. Only the decisions for the current time step are implemented, and the system state is updated before proceeding to the next iteration.

4.3. Scheduling module implementation

The Scheduling Module (SM) employs Soft Actor-Critic (SAC) reinforcement learning to enable adaptive real-time decision-making. The SAC algorithm is particularly well-suited for this application due to its ability to handle continuous action spaces and its maximum entropy framework, which encourages exploration while maintaining stable learning. The implementation initializes an actor network π_θ and two critic networks Q_{ϕ_1}, Q_{ϕ_2}, along with their corresponding target networks $Q_{\phi'_1}, Q_{\phi'_2}$. All networks employ three fully-connected hidden layers with dimensions [256, 256, 128] and ReLU activations. Target networks are updated via Polyak averaging, and the use of double Q-learning helps mitigate overestimation bias common in value-based methods.

During each episode, the environment is reset to an initial state s_0, and the agent interacts with the environment over the planning horizon. At each time step t, actions are sampled from the policy distribution $a_t \sim \pi_\theta(\cdot|s_t)$, where the policy outputs parameters of a squashed Gaussian distribution to ensure actions remain within valid bounds. After executing the action, the agent observes the reward r_t and next state s_{t+1}, storing the transition tuple (s_t, a_t, r_t, s_{t+1}) in a replay buffer for experience replay. The critics are updated by minimizing the mean squared Bellman error: $\mathcal{L}_Q = \mathbb{E}[(Q_\phi(s, a) - y)^2]$, where the target value is computed as $y = r + \gamma \cdot (\min(Q_{\phi'_1}, Q_{\phi'_2}) - \alpha \cdot \log \pi_\theta)$. The actor is updated to maximize the expected return while maintaining high entropy: $\mathcal{L}_\pi = \mathbb{E}[\alpha \cdot \log \pi_\theta(a|s) - Q_\phi(s, a)]$. The temperature parameter α is automatically adjusted to maintain a target entropy level through gradient descent on $\mathcal{L}_\alpha = \mathbb{E}[-\alpha \cdot (\log \pi_\theta(a|s) + \mathcal{H}_{\text{target}})]$.

4.4. Inter-layer coordination mechanism

The coordination between layers is implemented through a structured information exchange protocol that ensures consistency while respecting the computational constraints of each optimization method. The forward information flow follows a hierarchical pattern where each layer provides constraints and guidance to subsequent layers. The SLM communicates zone capacities C_z for each zone z, station locations loc_s for each station s, and the zone-station mapping $\mathcal{STA}_z \subseteq \mathcal{STA}$ to the RAM. Subsequently, the RAM provides vehicle-station assignments $X_{v,s,t}$, time window constraints $[t_{\text{start}}, t_{\text{end}}]$ for each assignment, and available power budget $P_{\text{available}}(t)$ to the SM.

Given the discrete nature of the optimization problems in the upper layers, traditional gradient-based feedback is infeasible. Instead, we implement a performance-based feedback mechanism that propagates aggregate metrics and constraint violations. The SM reports utilization metrics $u_{s,t}$ = actual usage/assigned capacity, violation indicators $v_{s,t}$ that signal constraint breaches, and performance scores $\rho_{s,t}$ computed as weighted combinations of efficiency metrics to the RAM. Similarly, the RAM communicates zone congestion indices $\text{CI}_z = \text{avg(utilization)} \times \text{avg(wait\_time)}$ and reallocation requests for zones requiring capacity adjustments to the SLM. This feedback mechanism enables each layer to adapt its decisions based on actual operational performance without requiring differentiability of the optimization algorithms.

4.5. Computational complexity and convergence analysis

The computational complexity of the framework varies significantly across layers due to their different optimization approaches and time scales. The SLM exhibits complexity of $\mathcal{O}(|\mathcal{Z}|^2 \cdot N_x \cdot N_y)$ for the Voronoi iteration process, with worst-case complexity of $\mathcal{O}(2^{|\mathcal{Z}|\cdot|\mathcal{G}|})$ for the ILP component, though modern solvers typically achieve much better performance through sophisticated branching strategies and cutting planes. The RAM complexity depends on the selected algorithm: MIP shows worst-case exponential complexity $\mathcal{O}(2^n)$ but typically performs at $\mathcal{O}(n^3)$ with good bounds, PSO exhibits $\mathcal{O}(N_p \cdot \text{max\_iter} \cdot \text{n})$ complexity, and RHH maintains $\mathcal{O}(T \cdot H \cdot |\mathcal{V}_t| \cdot |\mathcal{STA}_c|)$ complexity. The SM demonstrates complexity of $\mathcal{O}(|S| \cdot |\mathcal{A}| \cdot N_{\text{episodes}} \cdot T_{\text{episode}})$ for the learning phase, with inference complexity of $\mathcal{O}(|S|)$ for real-time decision-making.

The total framework complexity accounts for the different update frequencies of each layer: $T_{\text{total}} = T_{\text{SLM}}/\tau_{\text{SLM}} + T_{\text{RAM}}/\tau_{\text{RAM}} + T_{\text{SM}}/\tau_{\text{SM}} + T_{\text{coord}}$, where τ represents the update frequency for each layer. This multi-timescale approach ensures computational feasibility while maintaining system responsiveness. Convergence of the hierarchical framework is established through layer-wise guarantees: the SLM's ILP formulation guarantees optimal solutions within tolerance ϵ, the RAM achieves proven convergence to global optimum for MIP, probabilistic convergence to near-optimal solutions (typically 95–98% of optimal) for PSO, and bounded approximation ratio for RHH as demonstrated in Eq. (24). The SM's SAC algorithm convergence follows from maximum entropy reinforcement learning theory, with convergence rates dependent on the smoothness of the value function and the expressiveness of the function approximators.

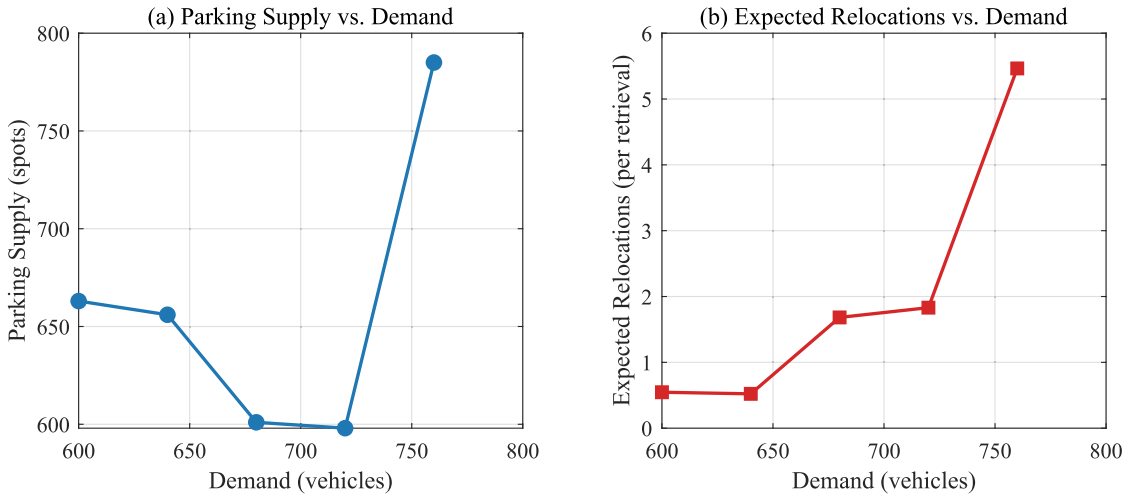

Fig. 5. Effect of demand on layout and performance.

4.6. Implementation considerations

The practical deployment of the framework requires careful attention to software architecture and operational constraints. The system employs a modular design with well-defined application programming interfaces (APIs) between layers, enabling independent development and testing of each component. Parallel execution is leveraged where possible, such as evaluating PSO particles concurrently or processing multiple charging stations simultaneously in the scheduling layer. Efficient data structures, including priority queues for vehicle scheduling and spatial indices for station proximity queries, are essential for maintaining real-time performance. To handle real-time constraints, the framework employs pre-computation and caching strategies for frequently accessed data, implements fail-safe mechanisms to handle solver timeouts gracefully, and utilizes incremental updates rather than full re-optimization when system changes are minor. These implementation details ensure that the theoretical framework translates effectively to practical deployment in commercial parking facilities.

5. Numerical experiments

We perform the following numerical experiments to gain managerial insights on EV charging operations and to assess the computational efficiency and accuracy of the proposed solution algorithms. The experiments adopt the real-time data collected from IoT-enabled parking facilities during January 2021 to June 2024 (John, 2024). The dataset comprises 1000 parking event records across 50 parking spots distributed in four zones, capturing comprehensive attributes including timestamps, vehicle types, parking duration, occupancy status, and environmental conditions. The vehicle composition consists of conventional cars (70.4%), motorcycles (19.1%), and electric vehicles (10.5%), with EVs accounting for 19.8% of total parking events. The parking duration follows a quasi-normal distribution with a mean of 2.87 hours (standard deviation: 1.63 hours), where approximately 48.5% of vehicles remain parked for 2–3 hours. Vehicle arrival patterns exhibit moderate temporal variations, with peak arrivals during afternoon (14:00-17:00) and evening periods (19:00-22:00). The average occupancy rate is 28.4%, ranging from 0.8% to 79.3%. Environmental parameters including temperature, precipitation, and traffic conditions are also recorded. Based on this dataset, we analyze the effect of demand on layout performance, investigate the impact of car-park dimensions, examine the influence of gap width, and compare the exact and heuristic frameworks.

5.1. Effect of demand on layout and performance

Consider a car-park with dimensions L = 150 [m], W = 65 [m], spot length l = 5 [m], and spot width w = 2 [m]. The car-park has y = 30 rows in each island and the width of the clearance roadway is 5 [m]. We increase the demand from D = 600 [veh] to D = 780 [veh] and examine the geometric shape of the optimal car-park layout.

Fig. 5 illustrates the effect of demand on parking supply and relocation costs. As shown in Fig. 5a, parking supply increases in a step-wise fashion. The points where the steps occur are the points where the layout changes significantly. For instance, from D = 0 to D = 660, the optimal layout consists of 20 two-column islands where the demand is evenly distributed among islands. At D = 661, however, the car-park layout changes substantially, leading to a jump in parking supply.

When demand is low to medium, the islands all have only two columns, which is similar to existing parking facilities for conventional vehicles. This two-column design has the lowest relocation cost and is preferable when demand is relatively low. As demand increases, the islands become larger with more columns. The two-column islands are eliminated at the highest demands because they

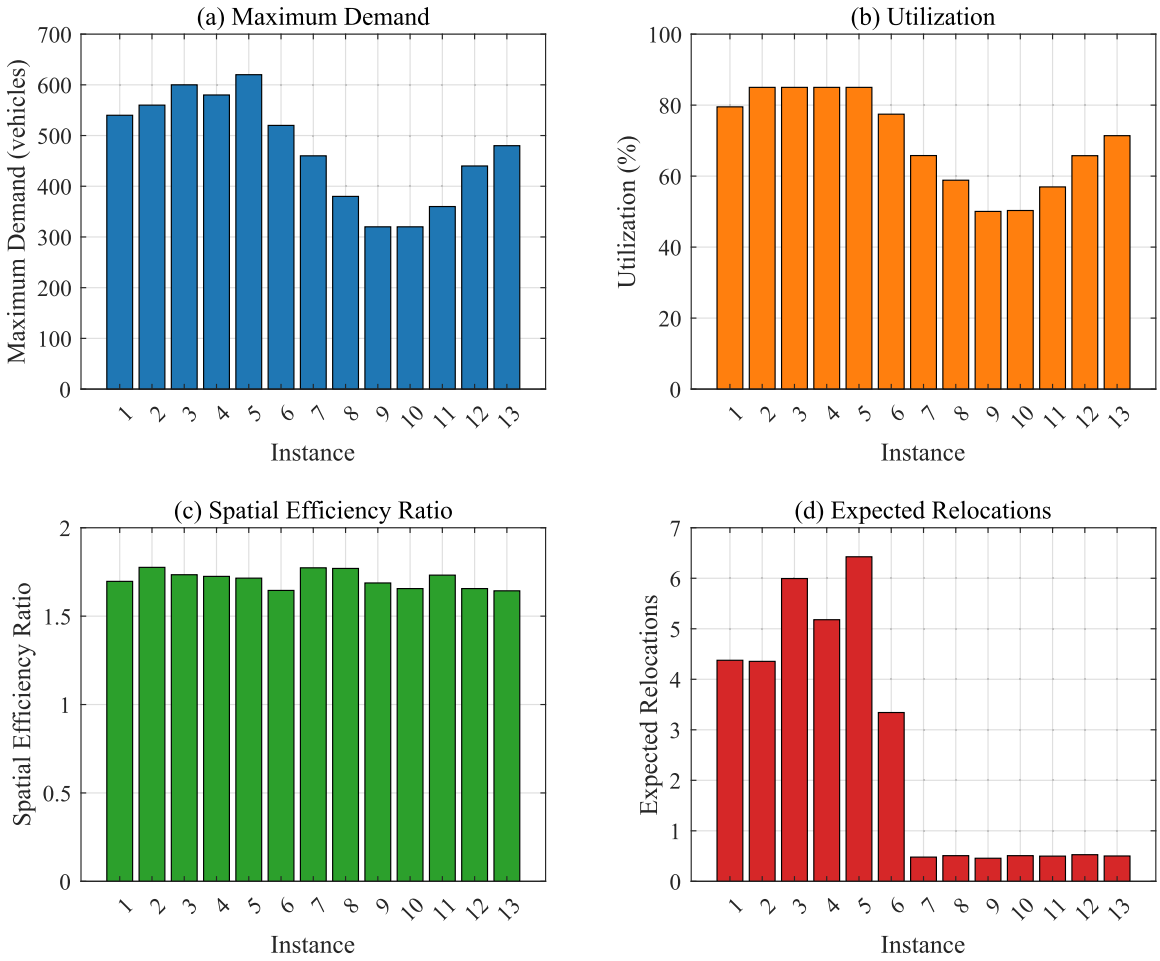

Fig. 6. Effect of car-park dimensions on performance metrics.

require gaps that occupy valuable land that could otherwise be used as island space. The maximum demand $D_{\max}$ that the car-park can serve is 780 [veh], with parking supply in the experimental scenarios being 660, 660, 720, 720, 780, and 780 vehicles, respectively.

Fig. 5b shows that expected relocations follow the same step-wise pattern with jumps occurring at layout transition points. There is also a gradual increase within each step, which is intuitive as higher demand requires more relocations. The results indicate that at the highest demand ($D = 780$ [veh]), approximately 5 vehicles must be relocated during any random retrieval operation.

5.2. *Effect of Car-Park dimensions on maximum demand*

The maximum demand $D_{\max}$ depends significantly on the area and dimensions of the car-park. We present 13 car-park instances in Fig. 6, each with different length L and width W but with identical total area (LW $= 6890$ [m^2]). Instances 1–13 represent different length-to-width ratios (L:W) while maintaining constant total area. The progression moves from elongated horizontal layouts through square configurations to elongated vertical layouts. The results show that the highest maximum demand, $D_{\max} = 560$, occurs in the square orientation where L $\approx$ W (Instance 7). This square orientation also demonstrates the lowest relocation cost among all instances, making it a particularly desirable configuration.

Fig. 6a and **b** illustrate that $D_{\max}$ and the utilization ratio are both generally higher in square orientations. The highest utilization ranges between 75% and 80% across all instances, indicating that approximately 80% of the land is allocated to parking spots and the remaining 20% to clearance roadway and inter-island gaps.

As shown in Fig. 6c, the spatial efficiency ratio averages 1.62 but can reach as high as 1.87, demonstrating that EV charging facilities can accommodate up to 87% more vehicles than conventional parking facilities. For car-parks with large width W, the spatial efficiency mainly derives from the smaller space requirements of each EV parking spot compared to conventional spots ($w = 2$ vs. $w = 2.8$). However, for car-parks with smaller width, the efficiency gain comes from both dimensional advantages and optimal vehicle relocation strategies.

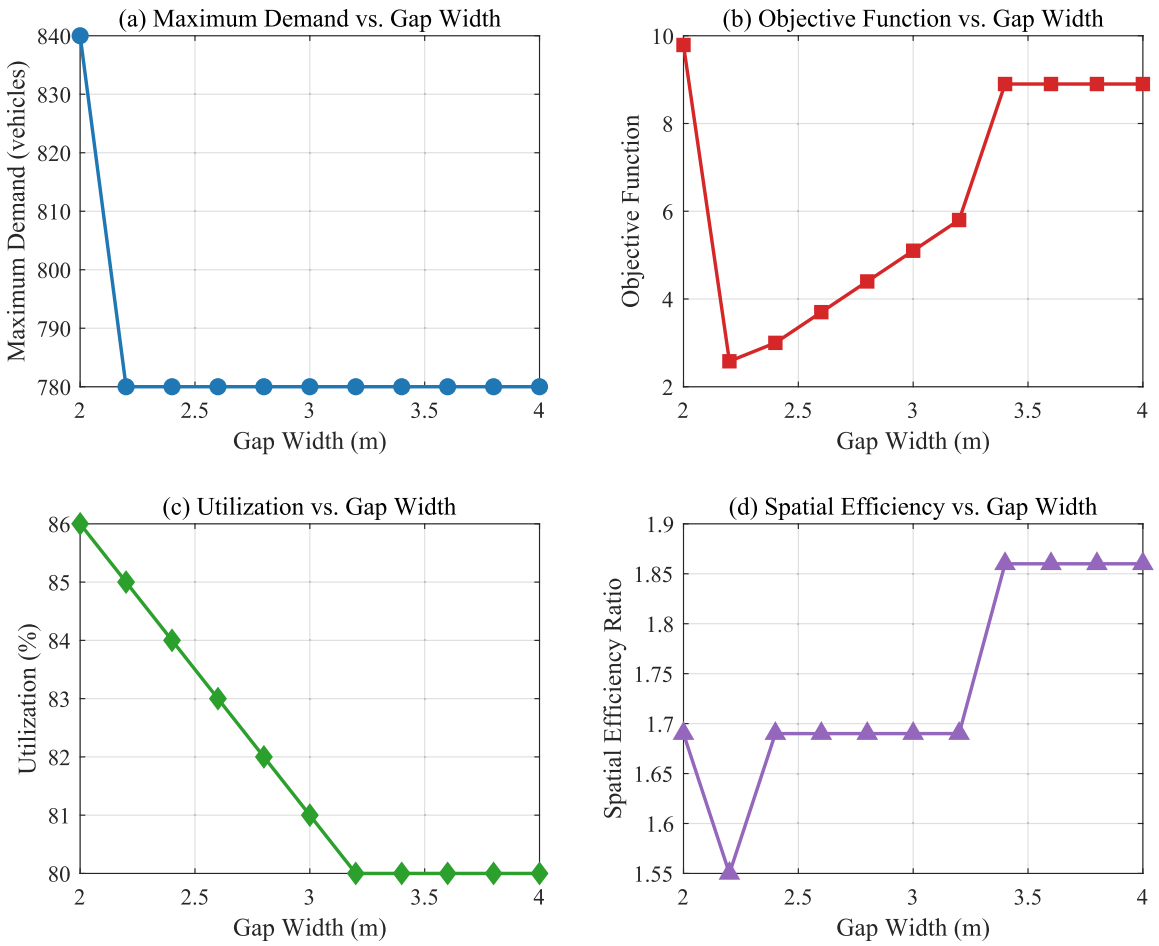

Fig. 7. Impact of gap width on layout performance. Instances 1–11 represent increasing gap widths from 2.0m to 4.0m in increments of 0.2m.

Fig. 6d plots relocation cost versus $D_{\max}$ for each instance, highlighting the Pareto efficiency achieved by square layouts, which balance maximum demand capacity with operational efficiency.

5.3. Impact of gap width on layout

We analyze the impact of gap width α on the optimal layout and performance of the car-park. Fig. 7 presents results for 11 instances with gap widths ranging from $\alpha = 2.0$ to $\alpha = 4.0$ m.

The utilization ratio decreases with increasing α, as shown in Fig. 7c, because wider gaps occupy more space, leaving less area available for parking islands. Consequently, the maximum demand $D_{\max}$ also decreases with α, as illustrated in Fig. 7a, since fewer vehicles can be accommodated in the car-park.

Interestingly, the objective function exhibits a non-monotonic pattern (Fig. 7b). There is an initial significant decrease from Instance 1 ($\alpha = 2.0$) to Instance 2 ($\alpha = 2.2$) because Instance 2 accommodates fewer vehicles. From Instance 2 onward, however, the objective function strictly increases despite serving the same demand ($D_{\max} = 780$ [veh]). This occurs because the layout becomes less efficient with increasing gap width, requiring more vehicle relocations.

Fig. 7d shows that the spatial efficiency ratio increases from 1.55 (Instance 2) to 1.86 (Instance 11) as α increases. This trend emerges because while $D_{\max}$ remains constant at 780 vehicles across Instances 2–11, the maximum capacity of a conventional two-column design decreases with wider gaps, thus increasing the relative advantage of the optimized layout.

5.4. Algorithm comparison - Exact vs. heuristic

We compare the performance of the exact and heuristic algorithms across 18 test instances with varying parameters. Fig. 8 illustrates the solution quality comparison, while Fig. 9 examines computational efficiency.

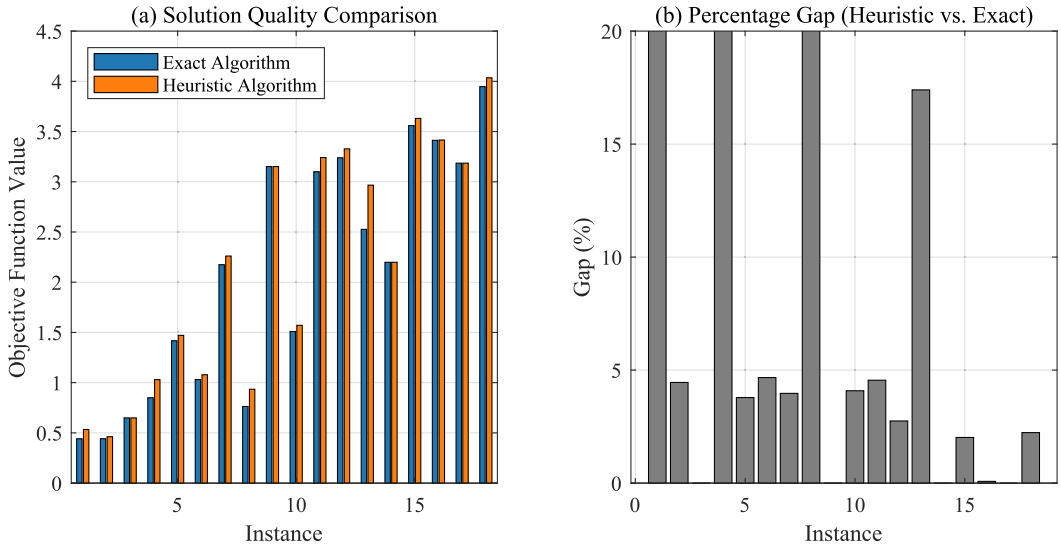

Fig. 8. Algorithm comparison - solution quality. Instances 1–18 represent test scenarios with varying combinations of car-park dimensions, demand levels, and gap widths.

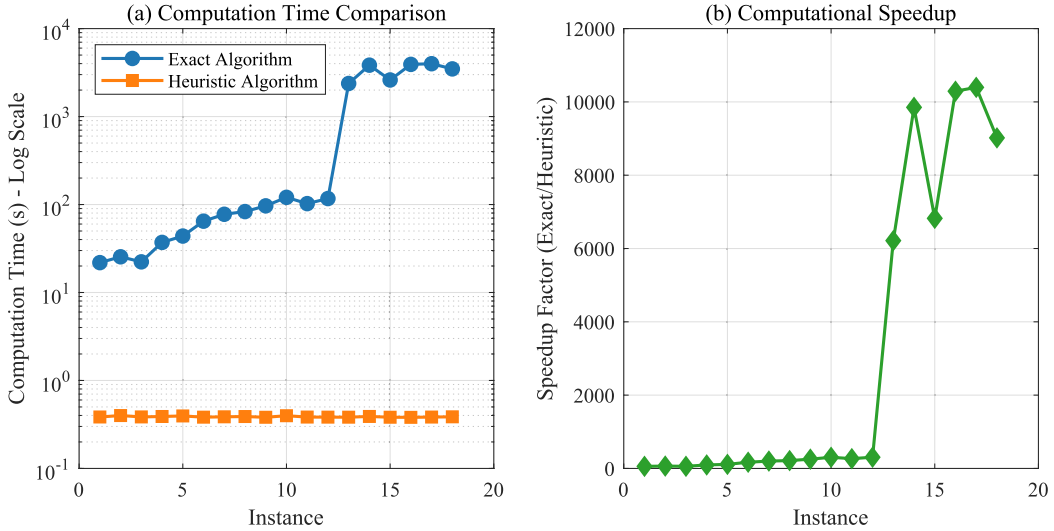

Fig. 9. Algorithm comparison - computational time. Instances correspond to the same test scenarios as Fig. 8, ordered by increasing problem complexity.

As shown in Fig. 8a, the objective function values obtained by the exact algorithm are consistently lower than or equal to those of the heuristic. The percentage gap in solution quality (Fig. 8b) ranges from 0% to 18%, with larger discrepancies occurring in instances with complex layout requirements where the exact algorithm can explore a wider range of configurations.

Fig. 9a presents computation time on a logarithmic scale, revealing that the exact algorithm requires significantly more processing time than the heuristic. The longest computation time occurs in Instance 15, requiring 5.3 hours for the exact algorithm but only 0.4 seconds for the heuristic. Fig. 9b shows the speedup factor (the ratio of exact to heuristic computation time), which ranges from 10× to over 40,000×, with larger speedups for more complex instances.

Fig. 10 provides a comprehensive view of the tradeoff between solution quality and computational efficiency. The bubble sizes represent problem complexity (area × demand), demonstrating that while the heuristic provides reasonable approximations for simpler problems, it may miss optimal solutions for more complex instances. In Instance 9, both algorithms yield identical objective values, but the exact algorithm requires 229.62 seconds compared to just 0.42 seconds for the heuristic, indicating that the heuristic can sometimes find optimal solutions with substantially reduced computational effort.

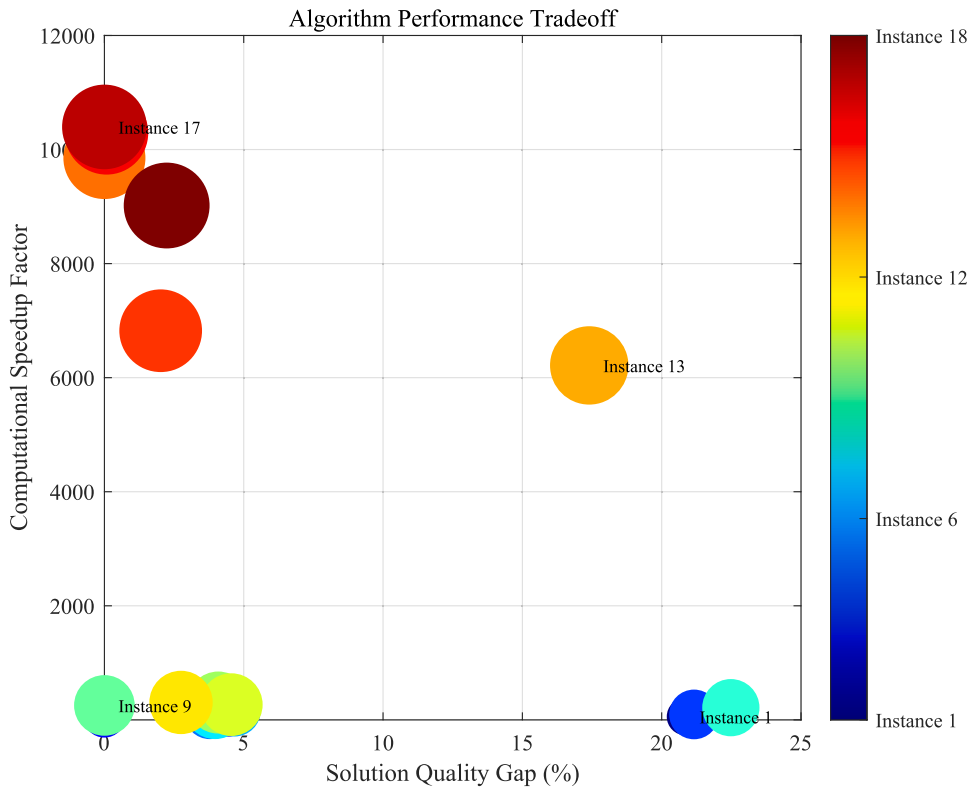

Fig. 10. Combined performance metric.

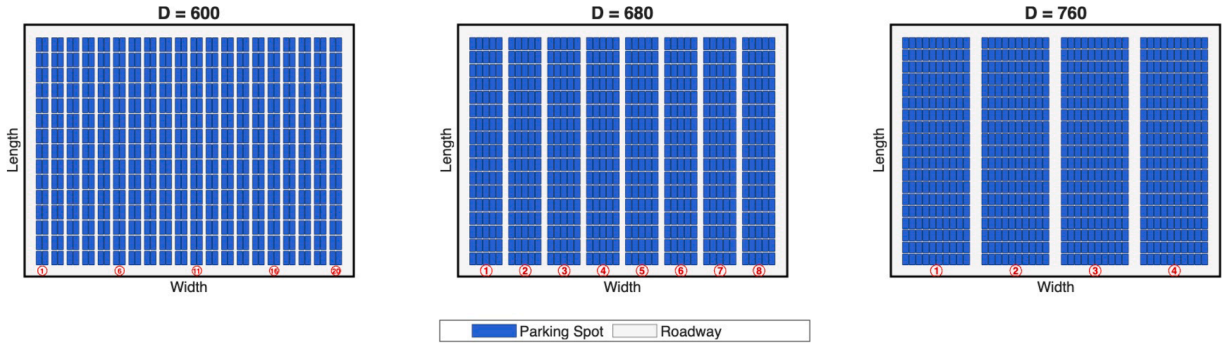

Fig. 11. Visualization of optimal layout for different demands.

5.5. *Visualization of optimal layouts*

Fig. 11 illustrates the optimal layouts for three demand scenarios ($D = 600$, 680, and 760). For D = 600, the layout consists of 20 two-column islands, similar to conventional parking facilities. As demand increases to D = 680, the layout transitions to 8 islands with more columns (5 columns per island). For the highest demand scenario ($D = 760$), the optimal design features just 4 islands with many columns (10–14 columns per island).

Fig. 12 presents a comprehensive comparison across all experiments. Fig. 12a contrasts utilization percentages between optimal and sub-optimal designs, while Fig. 12b compares efficiency metrics. The results consistently demonstrate that square-shaped car-parks with appropriate gap widths achieve the best overall performance, effectively balancing space utilization with operational efficiency.

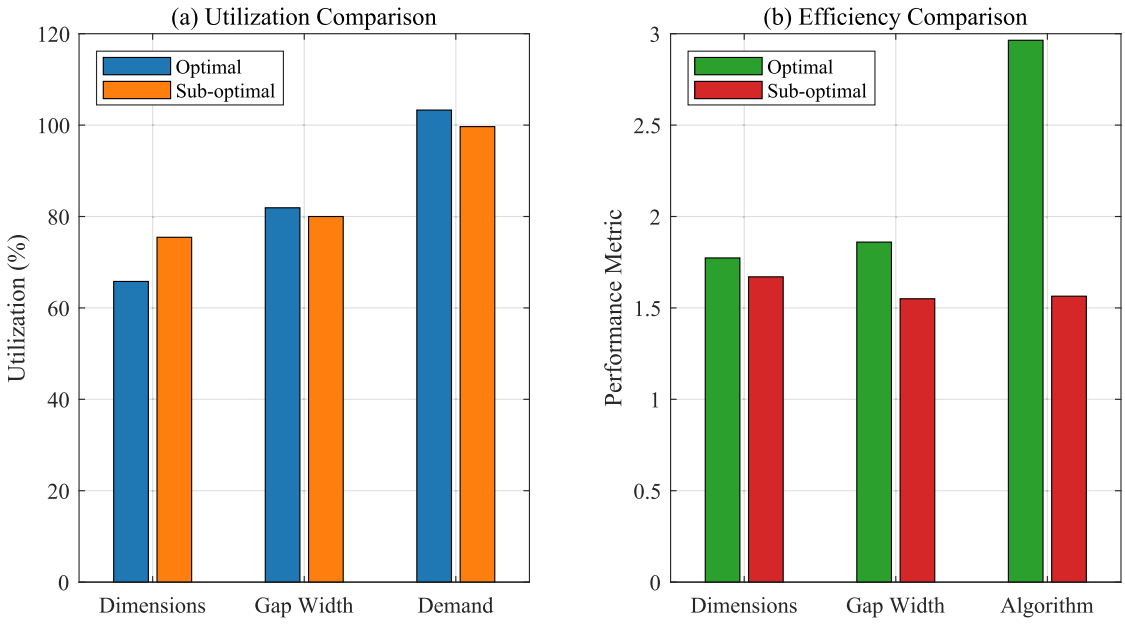

Fig. 12. Visualization of optimal layouts.

Table 3
Performance comparison of different optimization approaches.

Performance Metric	Traditional Approach	Single-Layer Optimization	Non-Coordinated Multi-Layer	Three-Layer Framework	Improvement (%)
Vehicle Movements (avg. per retrieval)	7.8	6.9	6.2	5.9	23.7
Charging Vehicles per Unit Time	183	196	211	222	21.4
Parking Occupancy Rate (%)	73.5	76.2	79.4	82.9	12.8
Average Waiting Time (min)	18.3	15.1	12.7	9.4	48.6
Energy Cost Reduction (%)	–	5.8	10.3	14.2	14.2
System Recovery Time (min)	47.2	38.4	29.5	21.6	54.2

5.6. Comprehensive performance evaluation

Table 3 presents a comprehensive performance comparison between our proposed three-layer framework and alternative approaches. The traditional approach represents current industry practices without optimization, while single-layer optimization focuses only on scheduling without considering spatial or resource allocation dimensions. The non-coordinated multi-layer approach implements all three layers but without the vertical and horizontal integration mechanisms described in Section 3.6. Across all metrics, our integrated three-layer framework demonstrates superior performance, with particularly significant improvements in system recovery time after failures (54.2% reduction) and average waiting time (48.6% reduction). The framework reduces vehicle movements by 23.7% compared to traditional approaches while increasing charging throughput by 21.4%. These findings align with but exceed the benefits observed in single-algorithm approaches such as the genetic algorithm implementation by (Zhou et al., 2022a; Hu et al., 2025b), highlighting the advantages of our integrated multi-layer architecture. Illmann and Kluge (2020), using Granger causality tests, discovered that increases in charging infrastructure lead to increases in EV registrations, rather than the reverse. This supports the fundamental premise of our framework-that by optimizing the configuration and operation of charging infrastructure, we can positively influence EV adoption and usage patterns. These results validate our hypothesis that addressing the interdependencies between spatial layout, resource allocation, and temporal scheduling yields substantial performance benefits beyond what can be achieved through isolated optimization of individual system components.

Table 4 evaluates the computational performance of our optimization framework under diverse operational conditions. Under normal operations, the system converges rapidly (3.7 seconds) with minimal optimality gap (1.8%), demonstrating high stability and adaptability. During peak demand periods with 150% normal load, convergence time increases to 6.2 seconds with a still acceptable 3.5% optimality gap. The framework demonstrates robust performance even under significant disruptions, such as 30% charging station failures, maintaining an adaptability index of 0.83. The system remains functional even during combined disruptions and extreme weather events, though with increased convergence time (15.3 seconds) and optimality gap (8.5%). The adaptability index-calculated as a weighted function of convergence speed, solution quality, and recovery capability-remains above 0.7 even in the

Table 4
Computational performance of the optimization framework.

Operational Scenario	Convergence Time(s)	Optimality Gap(%)	Adaptability Index
Normal Operations	3.7	1.8	0.94
Peak Demand	6.2	3.5	0.89
Charging Station Failures	8.4	5.2	0.83
Price Fluctuations	4.9	2.4	0.91
Combined Disruptions	12.7	7.1	0.78
Extreme Weather Event	15.3	8.5	0.72

most challenging scenarios, indicating the framework's resilience to operational disturbances. These results validate our theoretical stability analysis in Section 4.5 and demonstrate the practical robustness of our three-layer optimization approach under real-world conditions.

6. Discussion

Our three-layer optimization framework addresses fundamental challenges in EV charging management through the systematic integration of spatial, resource allocation, and temporal decision-making. The hierarchical architecture demonstrates that treating these traditionally isolated optimization domains within a unified framework yields substantial performance improvements beyond what single-layer approaches can achieve.

The 23.7% reduction in vehicle movements and 21.4% increase in charging throughput directly address the infrastructure utilization inefficiencies identified in our introduction. These improvements stem from the framework's ability to coordinate decisions across multiple time scales-strategic spatial planning, tactical resource allocation, and operational scheduling-rather than optimizing each domain independently. The 48.6% reduction in average waiting time particularly validates our hypothesis that integrated optimization better serves user experience while maintaining system efficiency. The stability enabling these performance gains is rooted in the validity of integrating decisions across vastly different time horizons. The justification lies in inherent interdependencies: strategic spatial decisions establish enduring physical constraints for operations, while long-term planning must be informed by operational realities to ensure infrastructure robustness. To prevent short-term operational fluctuations from destabilizing long-term strategies, the framework employs temporal decoupling with distinct update frequencies (SLM > RAM > SM). This ensures that faster operational layers reach a quasi-steady state before strategic layers adapt, aligning with singular perturbation theory, which guarantees bounded tracking error when fast and slow dynamics are adequately separated. Additionally, temporal filtering via exponential moving averages smooths performance metrics, ensuring that upper layers respond to sustained trends rather than transient fluctuations. Hysteresis bands around triggering thresholds further prevent chattering behavior. Finally, feedback between layers relies on aggregated key performance indicators rather than detailed operational data, allowing strategic layers to adapt based on systemic performance trends.

Regarding implementation, our adaptive algorithm selection strategy represents a key methodological contribution. By dynamically selecting between MIP, PSO, and RHH based on system complexity, the framework enables practical deployment across diverse facility scales. To address the trade-off between complexity and maintenance costs, the hierarchical design naturally mitigates computational bottlenecks through timescale decoupling. The computationally intensive Spatial Layout Module runs offline on a strategic horizon, effectively isolating it from real-time constraints. For resource-constrained environments, a 'lightweight' version can be implemented by locking the resource allocation module to the RHH ($O(n \log n)$). Furthermore, calibration complexity is managed by offloading heavy reinforcement learning training to cloud-based digital twins and deploying only the low-complexity inference model ($O(n)$) to local edge devices, ensuring the system remains robust and cost-effective.

Essential for practical deployment is the framework's resilience to stochastic and unexpected events, such as sudden reductions in available charging capacity due to grid instability or local equipment faults. Our hierarchical framework is specifically structured to absorb such shocks. A capacity reduction is immediately registered as a tightening of the system-level constraint. This change triggers a rapid re-evaluation at the resource allocation layer. The adaptive algorithm selection mechanism prioritizes the faster RHH or PSO to quickly determine a feasible allocation of the reduced capacity across all zones. This revised capacity constraint is then fed into the real-time scheduling layer as an updated state observation for the SAC agent. Since the SAC policy is trained on diverse scenarios, it can immediately issue a revised set of charging power commands that adhere to the new, tighter constraints, effectively mitigating the system impact by proportionally slowing down charging or re-sequencing the schedule to manage the reduced resource pool. Future work could focus on explicitly training the SAC agent to optimize for minimal disruption (by incorporating a "capacity loss penalty" into the reward function).

While the current implementation demonstrates significant efficacy, several avenues for enhancement remain. First, the framework focuses primarily on operational optimization within existing grid constraints; future iterations could incorporate more sophisticated demand forecasting models and dynamic pricing mechanisms (Bae et al., 2024). Second, integrating detailed mobility uncertainty models (Cao et al., 2018) could further enhance predictive accuracy beyond our current user behavior modeling. Finally, the current model relies solely on external grid capacity. Future research should explicitly model Vehicle-to-Vehicle (V2V) interactions, which

could augment the Resource Allocation Module by introducing neighboring vehicles as secondary power sources to overcome grid capacity bottlenecks during peak demand.

7. Conclusion

This research develops and validates a hierarchical three-layer optimization framework that fundamentally transforms electric vehicle charging infrastructure management. By systematically integrating spatial layout optimization, adaptive resource allocation, and real-time scheduling within a unified architecture, the framework addresses critical inefficiencies inherent in current charging management systems.

The bottom layer employs an integer linear programming approach to establish efficient zoned parking layouts, achieving spatial efficiency ratios of up to 1.87 and enabling EV facilities to accommodate 87% more vehicles than conventional parking configurations. The middle layer implements an adaptive algorithm selection mechanism that effectively balances solution quality with computational efficiency, providing scalable optimization across facility sizes ranging from small installations to large commercial complexes. The top layer incorporates reinforcement learning to enable continuous adaptation to evolving operational conditions while simultaneously optimizing multiple competing objectives.

Experimental validation demonstrates substantial performance improvements across all key metrics: 23.7% reduction in vehicle movements, 21.4% increase in charging throughput, 12.8% improvement in parking occupancy, and 14.2% reduction in electricity costs. These results validate our central hypothesis that coordinated multi-layer optimization delivers superior performance compared to isolated single-domain approaches. The framework's robust performance under operational stress-maintaining service during partial infrastructure failures and adapting to demand fluctuations-confirms its practical viability for commercial deployment.

As global EV adoption accelerates, this research addresses the critical need for intelligent infrastructure management by proposing a hierarchical optimization framework that systematically integrates spatial planning, resource allocation, and operational scheduling. Methodologically, this architecture captures the interdependencies between traditionally isolated decision domains , while practically, it provides a comprehensive solution balancing operational efficiency (Kim et al., 2023), user experience (Meyer et al., 2025), and economic performance (Lai et al., 2025). Validated through commercial implementation, the framework's modular design ensures adaptability to diverse contexts, offering a robust foundation for efficient, reliable, and economically viable electric mobility systems.

Future research should extend the framework to incorporate renewable energy integration (ElSayed et al., 2022) with stochastic forecasting (Wang et al., 2026; Hu et al., 2025c), alongside advanced bidirectional energy capabilities such as Vehicle-to-Grid (V2G) and Vehicle-to-Vehicle (V2V) trading. Specifically, V2V technology could enhance system capacity by utilizing high-SoC vehicles as localized energy buffers during grid congestion, building upon promising results demonstrated in residential settings (Nishanthy et al., 2023). Furthermore, scaling these operations to city-wide networks requires developing distributed optimization approaches for multi-facility coordination (Ju et al., 2022), while integrating game-theoretic properties (Nejad et al., 2017) represents a crucial theoretical advancement to ensure strategy-proofness for individual users within system-wide optimization.

CRediT authorship contribution statement

Zi-Xuan Zhou: Writing – review & editing, Writing – original draft, Validation, Methodology, Data curation, Conceptualization; **Jiawei Feng:** Visualization, Software, Resources, Conceptualization; **Haowen Lei:** Visualization, Software, Data curation; **Wenjun Mei:** Validation, Supervision, Methodology, Formal analysis, Data curation; **Yasuo Asakura:** Visualization, Supervision, Software, Resources; **Kai Liu:** Writing – review & editing, Visualization, Validation, Supervision, Software, Resources, Funding acquisition, Data curation.

Declaration of competing interest

The authors declare that they have no known competing financial interests or personal relationships that could have appeared to influence the work reported in this paper.

Acknowledgements

This work was supported by the National Natural Science Foundation of China (72471045, 72595832). We also acknowledge the support of computing resources provided by the High-performance Computing Platform of Peking University.

References

Amirteimoori, A., Kia, R., Mohamed, M., Weber, G.-W., 2025. An innovative framework integrating MILP and a parallel optimal algorithm for UAV-enabled last-mile delivery. Int. J. Prod. Res. 0 (0), 1–21.

An, K., 2020. Battery electric bus infrastructure planning under demand uncertainty. Transp. Res. Part C: Emerging Technologies 111, 572–587.

Babar, Y., Burtch, G., 2024. Recharging retail: estimating consumer demand spillovers from electric vehicle charging stations. Manufacturing Service Oper. Manag. 26 (3), 797–813.

Bae, S., Kulcsár, B., Gros, S., 2024. Personalized dynamic pricing policy for electric vehicles: reinforcement learning approach. Transp. Res. Part C: Emerging Technologies 161, 104540.

Basso, R., Kulcsár, B., Sanchez-Diaz, I., et al., 2021. Electric vehicle routing problem with machine learning for energy prediction. Transp. Res. Part B 145, 24–55.

Boyacıl, B., Zografos, K.G., Geroliminis, N., et al., 2015. An optimization framework for the development of efficient one-way car-sharing systems. Eur. J. Oper. Res. 240 (3), 718–733.
Broadbent, G.H., Allen, C.I., Wiedmann, T., Metternicht, G.I., et al., 2022. Accelerating electric vehicle uptake: modelling public policy options on prices and infrastructure. Transp. Res. Part A 162, 155–174.
Cao, Y., Wang, T., Kaiwartya, O., Min, G., Ahmad, N., Abdullah, A.H., et al., 2018. An EV charging management system concerning drivers' trip duration and mobility uncertainty. IEEE Trans. Syst., Man, Cybern. 48 (4), 596–607.
Chen, G., Yang, L., Cao, X., et al., 2025. A deep reinforcement learning-based charging scheduling approach with augmented lagrangian for electric vehicles. Appl. Energy 378, 124706.
Chung, S.H., Kwon, C., 2015. Multi-period planning for electric car charging station locations: a case of korean expressways. Eur. J. Oper. Res. 242 (2), 677–687.
Davatgari, A., Cokyasar, T., Subramanyam, A., Larson, J., Mohammadian, A.K., et al., 2024. Electric vehicle supply equipment location and capacity allocation for fixed-route networks. Eur. J. Oper. Res. 317 (3), 953–966.
Davis, S.J., Lewis, N.S., Shaner, M., Aggarwal, S., Arent, D., Azevedo, I.L., Benson, S.M., Bradley, T., Brouwer, J., Chiang, Y.-M., Clack, C. T.M., Cohen, A., Doig, S., Edmonds, J., Fennell, P., Field, C.B., Hannegan, B., Hodge, B.-M., Hoffert, M.I., Ingersoll, E., Jaramillo, P., Lackner, K.S., Mach, K.J., Mastrandrea, M., Ogden, J., Peterson, P.F., Sanchez, D.L., Sperling, D., Stagner, J., Trancik, J.E., Yang, C.-J., Caldeira, K., et al., 2018. Net-zero emissions energy systems. Science 360 (6396).
Dolgui, A., Kovalev, S., Kovalyov, M.Y., et al., 2025. Scheduling electric vehicle regular charging tasks: a review of deterministic models. Eur. J. Oper. Res. 325 (2), 221–232.
ElSayed, M., Foda, A., Mohamed, M., 2022. Autonomous drone charging station planning through solar energy harnessing for zero-emission operations. Sustain. Cities Soc. 86, 104122.
Foda, A., Mohamed, M., 2026. Zero-emission medium- and heavy-duty fleet operation: the perspectives of stakeholders. Transp. Res. Part D 150, 105127.
Ghamami, M., Kavianipour, M., Zockaie, A., Hohnstadt, L.R., Ouyang, Y., et al., 2020. Refueling infrastructure planning in intercity networks considering route choice and travel time delay for mixed fleet of electric and conventional vehicles. Transp. Res. Part C: Emerging Technologies 120, 102802.
Habib, S., Ahmad, F., Gulzar, M.M., Ahmed, E.M., Bilal, M., et al., 2025. Electric vehicle charging infrastructure planning model with energy management strategies considering ev parking behavior. Energy 316, 134421.
He, S.Y., Kuo, Y.-H., Sun, K.K., 2022. The spatial planning of public electric vehicle charging infrastructure in a high-density city using a contextualised location-allocation model. Transp. Res. Part A 160, 21–44.
He, Y., Liu, Z., Song, Z., 2020. Optimal charging scheduling and management for a fast-charging battery electric bus system. Transp. Res. Part E 142, 102056.
Hiermann, G., Puchinger, J., Ropke, S., Hartl, R.F., et al., 2016. The electric fleet size and mix vehicle routing problem with time windows and recharging stations. Eur. J. Oper. Res. 252 (3), 995–1018.
Hu, X., Chen, F., Sun, H., 2025a. Optimization of urban parking cooperation and pricing: a case of harbin, china. Transp. Res. Interdiscip. Perspect. 33, 101619.
Hu, X., Qiu, Z., Gao, W., 2025b. Optimization of electric bus dispatching interval considering stochastic traffic conditions. Transp. Lett. 17 (2), 200–213.
Hu, X., Qiu, Z., Wang, H., Gao, W., 2025c. Optimization of electric bus scheduling: with the consideration of stochastic traffic conditions. Transp. Plan. Technol. 0 (0), 1–24.
Iacobucci, R., McLellan, B., Tezuka, T., 2019. Optimization of shared autonomous electric vehicles operations with charge scheduling and vehicle-to-grid. Transp. Res. Part C: Emerging Technologies 100, 34–52.
Illmann, U., Kluge, J., 2020. Public charging infrastructure and the market diffusion of electric vehicles. Transp. Res. Part D 86, 102413.
Jin, J., Xu, Y., 2021. Optimal policy characterization enhanced actor-critic approach for electric vehicle charging scheduling in a power distribution network. IEEE Trans. Smart. Grid. 12 (2), 1416–1428.
John, A.B., 2024. Smart parking management dataset. https://www.kaggle.com/dsv/9686139. https://doi.org/10.34740/KAGGLE/DSV/9686139
Jordán, J., Palanca, J., Martí, P., Julian, V., et al., 2022. Electric vehicle charging stations emplacement using genetic algorithms and agent-based simulation. Expert Syst. Appl. 197, 116739.
Ju, Y., Liu, W., Zhang, Z., Zhang, R., et al., 2022. Distributed three-phase power flow for AC/DC hybrid networked microgrids considering converter limiting constraints. IEEE Trans Smart Grid 13 (3), 1691–1708.
Kim, J., Tak, S., Lee, J., Yeo, H., et al., 2023. Integrated design framework for on-demand transit system based on spatiotemporal mobility patterns. Transp. Res. Part C: Emerging Technologies 150, 104087.
Kinay, Ö.B., Gzara, F., Alumur, S.A., 2021. Full cover charging station location problem with routing. Transp. Res. Part B 144, 1–22.
Lai, Z., Shang, Y., Dong, T., Li, S., et al., 2025. Integrating valet charging with mobile discharging services: a strengthened integer L-shaped method. Transp. Sci. , trsc.2024.0912.
Liu, X., Plötz, P., Yeh, S., Liu, Z., Liu, X.C., Ma, X., 2024. Transforming public transport depots into profitable energy hubs. Nat. Energy .
Ma, X., Ma, W., Tao, Y., Gao, K., Liu, X., 2025. Optimizing bus charging infrastructure by incorporating private car charging demands and uncertain solar photovoltaic generation. npj Sustain. Mobil. Transp. 2, 6.
Mahyari, E., Freeman, N., 2025. Electric vehicle fleet charging management: an approximate dynamic programming policy. Eur. J. Oper. Res. 327 (1), 263–279.
Meyer, A., Gschwind, T., Amberg, B., Colling, D., et al., 2025. Exact algorithms for routing electric autonomous mobile robots in intralogistics. Eur. J. Oper. Res. 323 (3), 830–851.
Najafi, A., Gao, K., Parishwad, O., Tsaousoglou, G., Jin, S., Yi, W., et al., 2025. Integrated optimization of charging infrastructure, electric bus scheduling and energy systems. Transp. Res. Part D 141, 104664.
Nejad, M.M., Mashayekhy, L., Chinnam, R.B., Grosu, D., et al., 2017. Online scheduling and pricing for electric vehicle charging. IISE Trans. 49 (2), 178–193.
Nishanthy, J., Charles Raja, S., Jeslin Drusila Nesamalar, J., et al., 2023. Feasibility analysis of solar PV system in presence of EV charging with transactive energy management for a community-based residential system. Energy Convers. Manage. 288, 117125.
Nolz, P.C., Absi, N., Feillet, D., Seragiotto, C., 2022. The consistent electric-vehicle routing problem with backhauls and charging management. Eur. J. Oper. Res. 302 (2), 700–716.
Nourinejad, M., Bahrami, S., Roorda, M.J., et al., 2018. Designing parking facilities for autonomous vehicles. Transp. Res. Part B 109, 110–127.
Park, H., Lee, C., 2024. An exact algorithm for maximum electric vehicle flow coverage problem with heterogeneous chargers, nonlinear charging time and route deviations. Eur. J. Oper. Res. 315 (3), 926–951.
Powell, S., Cezar, G.V., Min, L., Azevedo, I. M.L., Rajagopal, R., et al., 2022. Charging infrastructure access and operation to reduce the grid impacts of deep electric vehicle adoption. Nat. Energy 7 (10), 932–945.
Qiu, Z., Hu, X., An, S., 2026. Robust collaborative scheduling optimization for multiple electric bus routes under stochastic traffic conditions. Transp. Res. Part C: Emerging Technologies 182, 105455.
Stephan, K., Weidinger, F., Boysen, N., 2021. Layout design of parking lots with mathematical programming. Transp. Sci. 55 (4), 930–945.
Sun, X., Chen, Z., Yin, Y., et al., 2020. Integrated planning of static and dynamic charging infrastructure for electric vehicles. Transp. Res. Part D 83, 102331.
Tang, X., Lin, X., He, F., 2019. Robust scheduling strategies of electric buses under stochastic traffic conditions. Transp. Res. Part C 105, 163–182.
Tang, Z.-Y., Tian, L.-J., Liu, P., Huang, H.-J., et al., 2025. Parking reservation scheme in a commuting system with shared autonomous vehicles and parking space constraint. Transp. Res. Part B 192, 103116.
Tran, C.Q., Keyvan-Ekbatani, M., Ngoduy, D., Watling, D., 2021. Stochasticity and environmental cost inclusion for electric vehicles fast-charging facility deployment. Transp. Res. Part E 154, 102460.
Unterluggauer, T., Rich, J., Andersen, P.B., Hashemi, S., et al., 2022. Electric vehicle charging infrastructure planning for integrated transportation and power distribution networks: a review. eTransportation 12, 100163.
Wang, W., Mohamed, M., Zhang, B., Zhang, Q., Abdelaty, H., 2026. Electric bus energy prediction and factors interactions using explainable machine learning models. Eng. Appl. Artif. Intell. 163, 112877.

Wang, W., Zhao, J., 2023. Partial linear recharging strategy for the electric fleet size and mix vehicle routing problem with time windows and recharging stations. Eur. J. Oper. Res. 308 (2), 929–948.
Wu, Y., Hu, X., Wang, Y., Jiang, Y., 2025. Assessing and mitigating carbon emission exposure in dynamic multimodal transport networks. Sustain. Cities Soc. 133, 106852.
Xie, F., Liu, C., Li, S., Lin, Z., Huang, Y., 2018. Long-term strategic planning of inter-city fast charging infrastructure for battery electric vehicles. Transp. Res. Part E 109, 261–276.
Xu, M., Meng, Q., 2020. Optimal deployment of charging stations considering path deviation and nonlinear elastic demand. Transp. Res. Part B 135, 120–142.
Xu, Y., Çolak, S., Kara, E.C., Moura, S.J., González, M.C., et al., 2018. Planning for electric vehicle needs by coupling charging profiles with urban mobility. Nat. Energy 3 (6), 484–493.
Yan, Y., Wen, H., Deng, Y., Chow, A. H.F., Wu, Q., Kuo, Y.-H., 2024. A mixed-integer programming-based q-learning approach for electric bus scheduling with multiple termini and service routes. Transp. Res. Part C: Emerging Technologies 162, 104570.
Yang, S.Y., Woo, J., Lee, W., 2024. Assessing optimized time-of-use pricing for electric vehicle charging in deep vehicle-grid integration system. Energy Econ. 138, 107852.
Yang, X., Niu, D., Sun, L., Ji, Z., Zhou, J., Wang, K., Siqin, Z., 2021. A bi-level optimization model for electric vehicle charging strategy based on regional grid load following. J Clean Prod 325, 129313.
Zaidi, I., Oulamara, A., Idoumghar, L., Basset, M., et al., 2024. Minimizing grid capacity in preemptive electric vehicle charging orchestration: complexity, exact and heuristic approaches. Eur. J. Oper. Res. 312 (1), 22–37.
Zhang, L., Wang, S., Qu, X., 2021. Optimal electric bus fleet scheduling considering battery degradation and non-linear charging profile. Transp. Res. Part E 154, 102445.
Zhao, Z., Lee, C. K.M., Yan, X., Wang, H., 2024. Reinforcement learning for electric vehicle charging scheduling: a systematic review. Transp. Res. Part E 190, 103698.
Zhou, G., Zhu, Z., Luo, S., et al., 2022a. Location optimization of electric vehicle charging stations: based on cost model and genetic algorithm. Energy 247, 123437.
Zhou, X., Meng, Q., Ji, Y., 2025. Optimal charging schedules for EV charging stations considering hybrid smart and uncontrolled charging: a scalable framework. Appl. Energy 398, 126366.
Zhou, Y., Meng, Q., Ong, G.P., et al., 2022b. Electric bus charging scheduling for a single public transport route considering nonlinear charging profile and battery degradation effect. Transp. Res. Part B 159, 49–75.
Zhou, Y., Meng, Q., Ong, G.P., Wang, H., 2024. Electric bus charging scheduling on a bus network. Transp. Res. Part C 161, 104553.